Spatial scale and distribution of neurovascular signals underlying decoding of orientation and eye-of-origin from fMRI data

Jonas Larsson[1], Charlotte Harrison, Jade Jackson, Seung-Mock Oh, and Vaida Zeringyte

[1]Corresponding author

Department of Psychology, Royal Holloway, University of London
Egham, TW20 0EX United Kingdom

jonas.larsson@rhul.ac.uk
+44 1784 414061

Abstract

Multivariate pattern analysis of functional MRI (fMRI) data is widely used, yet the spatial scales and origin of neurovascular signals underlying such analyses remain unclear. We compared decoding performance for stimulus orientation and eye-of-origin from fMRI measurements in human visual cortex with predictions based on the columnar organisation of each feature, and estimated the spatial scales of patterns driving decoding.

Both orientation and eye-of-origin could be decoded significantly above chance in early visual areas (V1-V3). Contrary to predictions based on a columnar origin of response biases, decoding performance for eye-of-origin in V2 and V3 was not significantly lower than that in V1, nor did decoding performance for orientation and eye of origin differ significantly. Instead, response biases for both features showed large-scale organization, evident as a radial bias for orientation, and a nasotemporal bias for eye preference.

To determine whether these patterns could drive classification, we quantified the effect on classification performance of binning voxels according to visual field position. Consistent with large-scale biases driving classification, binning by polar angle yielded significantly better decoding performance for orientation than random binning in V1-V3. Similarly, binning by hemifield significantly improved decoding performance for eye-of-origin. Patterns of orientation and eye preference bias in V2 and V3 showed a substantial degree of spatial correlation with the corresponding patterns in V1, suggesting that response biases in these areas originate in V1.

Together, these findings indicate that multivariate classification results need not reflect the underlying columnar organization of neuronal response selectivities in early visual areas.

New & Noteworthy

- Large-scale response biases can account for decoding of orientation and eye-of-origin in human V1-V3
- For eye-of-origin this pattern is a nasotemporal bias; for orientation it is a radial bias
- Differences in decoding performance across areas and stimulus features are not well predicted by differences in columnar-scale organisation of each feature
- Large-scale biases in extrastriate areas are spatially correlated with those in V1, suggesting biases originate in primary visual cortex

Keywords

Multivariate pattern classification analysis
Functional magnetic resonance imaging
Ocular dominance columns
Orientation columns
Human visual cortex
Primary visual cortex
Extrastriate visual cortex

Introduction

Multivariate pattern analysis and classification techniques (MVPA) have become widely used for analysis of fMRI data, owing largely to their high sensitivity compared to conventional mass univariate methods in combination with their ability to detect changes in voxel activity patterns even in the absence of overall changes in mean activity across voxels (Haxby et al., 2001). Despite the widespread use of such techniques, the origin of the signals which MVPA relies on remains unclear, both with regard to the spatial scale of the underlying signals, and whether these signals reflect neuronal or vascular responses. Although it was originally proposed that the response biases driving classification are due to biased sampling of columnar structures at smaller scales than voxels (Haynes and Rees, 2005; Kamitani and Tong, 2005), this assumption has been challenged by more recent studies showing the existence of large-scale patterns of response bias for orientation (Freeman et al., 2011, 2013) and motion direction (Beckett et al., 2012), which can account for decoding these features. Similarly, it has been hypothesized (Shmuel et al., 2010) that decoding of eye-of-origin could rely on a large-scale preference for the contralateral eye found in non-human primates (Horton and Hocking, 1996; Tychsen and Burkhalter, 1997), but this conjecture has not been explicitly tested. It is not known whether a similar nasotemporal bias exists also in human V1, although a possibly related large-scale preference for left over right eye stimulation was reported by Schwarzkopf et al. (2010). Despite the evidence for the existence of large-scale biases, their importance for classification remains a matter of considerable debate. Alink et al. (2012) showed that stimulus orientation can be decoded in the absence of global biases, suggesting radial biases might be induced by the choice of stimulus; in a similar vein but using a purely modelling-based approach, Carlson (2014) suggested that response biases might be driven by activity elicited by stimulus edges. Swisher et al. (2010), using a multiscale analysis, found that information about stimulus orientation was primarily found at scales of several millimeters, with only relatively small contributions from larger (>1cm) scales. Similarly, Shmuel et al. (2010) reported that at high field strengths (7T), information about the stimulated eye exists at multiple spatial scales. Meanwhile, other studies have shown that MVPA is robust to spatial smoothing, which has been interpreted as evidence against a columnar-scale bias driving classification (Op de Beeck, 2010) (although see Kamitani and Sawahata (2010) for an alternative interpretation of this result). A problem with the idea that MVPA relies on columnar biases is that computational analyses show that due to the way MRI data is acquired, response biases at sub-voxel (columnar) scales should not

be detectable at the resolution commonly used by most MVPA studies (about 3mm isotropic) (Chaimow et al., 2011). In addition, the assumption that the response biases reflect neuronal response properties has been called into question by results suggesting such biases may be vascular in origin (Gardner, 2010; Shmuel et al., 2010).

The uncertainty about the origin of signals underlying MVPA renders interpretation of results from such studies potentially problematic, especially when the techniques are used to identify cortical regions selective for particular stimulus features, as this approach depends on the assumption that the signals driving classification reflect neuronal responses in the areas under measurement. Verifying this assumption is thus of critical importance for establishing the validity of using MVPA for studying cortical function and organization. Although the problem of inferring neuronal response properties from BOLD fMRI signals is not unique to MVPA approaches, quantitative interpretation of MVPA results is made particularly difficult by the complex dependence of decoding performance on the spatial distribution of BOLD responses (Chaimow et al., 2011).

One potential strategy for addressing this issue is to compare results obtained by MVPA with predictions based on the known physiology of the two most well-defined columnar-scale structures in early visual cortex, ocular dominance and orientation columns, both of which have been reported in human V1 (Cheng et al., 2001; Adams et al., 2007; Yacoub et al., 2007, 2008). Because these two columnar structures differ in spatial organization and, in the case of ocular dominance columns, are restricted to V1, they make specific and potentially testable predictions about how decoding performance for orientation and eye-of-origin should differ within and between visual areas. First, if columnar signals underlie decoding, then decoding performance for eye-of-origin in extrastriate areas (which lack ocular dominance columns and monocular neurons [Hubel and Livingstone, 1987; Tootell and Hamilton, 1989; T'so et al. 1990; Adams et al. 2007; Nasr et al., 2016]) should be significantly lower than in V1. Second, if decoding depends solely on columnar-scale information, the differences in spatial organization between orientation and ocular dominance columns predict differences in decoding performance (Shmuel at al., 2010; Chaimow et al., 2011). Ocular dominance columns are anisotropic, forming elongated slabs or stripes up to several centimeters long, whereas orientation columns are relatively isotropic and iso-orientation domains rarely extend over more than 1 mm in any direction (Blasdel 1992; Obermayer and Blasdel 1993; Adams et al. 2007; Yacoub et al., 2007,

2008; Shmuel et al., 2010). Because draining veins are elongated, they are more likely to drain disproportionately from a single ocular domain than a single orientation domain (Shmuel at al., 2010). In the absence of any coarser scale information, this would predict that vascular signals should be more strongly dominated by eye preference than orientation preference. (Smith et al., 2011). Provided that the BOLD responses to orientation and eye stimulation were equal (since BOLD response magnitude strongly influences decoding [Smith et al;, 2011], this should in principle translate into higher decoding performance for eye-of-origin than for orientation. While direct measurements of columnar responses at high field strength (7T) have found similar magnitudes of response differences to orthogonal orientations and different eyes (Yacoub et al., 2007, 2008), differences in stimuli and experimental setup preclude a direct comparison across previous studies that have only considered ocular dominance or orientation in isolation. In this study we have investigated the spatial scale of signals driving decoding of both orientation and eye-of-origin. By using the same stimuli and data for both features, we were able to compare classification performance of these two features to determine whether the results of decoding matched predictions based on the different columnar-scale organisation of these features. We explored the alternative hypothesis that MVPA relies on large-scale spatial patterns by identifying any large-scale patterns in response biases for orientation and eye preference and testing if such patterns could account for classification of the two features. Specifically, we tested whether orientation decoding could be accounted for by a radial bias, as suggested by a previous study (Freeman et al., 2011), and whether decoding of eye-of-origin could be driven by a nasotemporal bias in V1 similar to that found in non-human primates (Horton and Hocking, 1996; Tychsen and Burkhalter, 1997). Briefly, our results show that both stimulus features exhibit large-scale patterns of response bias, neither of which are well explained by irregular sampling of the underlying columnar structures. For orientation, this large-scale pattern corresponds to the bias for radial orientations demonstrated by several previous studies (Sasaki et al., 2006; Clifford et al., 2009; Freeman et al., 2011), while for eye-of-origin the pattern is evident as a nasotemporal bias reflecting preference for the contralateral eye. Arguing against a columnar origin as the basis of classification for these features, we found that both of these large-scale patterns could account for decoding; moreover, decoding performance for the two features only incompletely matched predictions based on differences in columnar-scale structures for orientation and eye preference in V1 and extrastriate visual areas. Furthermore, the large-scale patterns of response biases in extrastriate areas V2

and V3 were spatially correlated with those in V1, suggesting that the biases in extrastriate cortex originate in V1. These results imply that MVPA can be driven by large-scale patterns that may not directly reflect neuronal response selectivities measured by single-unit recordings at columnar scales, which has important implications for using MVPA to map functional organization of the human brain with fMRI.

Materials and methods

Five subjects (two males) aged between 19 and 24 took part in the study. All except one (S2) were naïve to the purpose of the experiments. Subjects gave informed consent to participate in accordance with safety guidelines for MRI experiments (Kanal et al., 2002) and the experiments were approved by the local research ethics committee.

Stimuli and experimental conditions

For the main experiment, stimuli consisted of 1 cpd grayscale sinusoidal gratings presented in an annulus (inner and outer radii 1.5 and 6 degrees respectively) around fixation against a uniform gray background. The dimensions of the stimuli were chosen to ensure that no part of the grating intersected the blind spot of any of the subjects. Stimuli were presented dichoptically by frame-sequential presentation at 85Hz using the Nordic Neurolab fMRI-compatible goggle system with a display resolution of 800 x 600 pixels. Stimulus presentation and response recording was performed with custom software (MGL) written in Matlab (Mathworks, Natick, MA) and C. Gratings were shown to only one eye at a time, the other eye viewing a uniform gray background with the same mean luminance as the grating. Gratings were shown at 100% contrast at one of four different orientations (0, 45, 90, and 135 degrees from horizontal) to each eye, resulting in a total of eight trial types (corresponding to stimulus conditions). Each trial consisted of continuous presentation of a grating stimulus at one orientation shown either to the left or right eye for 6 s, randomly changing spatial phase every 0.1 s (Fig 1A). Consecutive trials were separated by intervals varying randomly in duration between 12 to 24s in steps of 1.5s, during which a uniform gray background was shown to both eyes. Trial and intertrial durations were even multiples of the scan repetition time (TR=1.5 s) such that stimulus presentation was always synchronized with scanner data acquisition. Each stimulus condition was repeated four times per run and there were a total of five runs per subject, yielding 20 repeats of each stimulus condition per subject. Trial order was permuted semi-randomly within each run, such that each trial was equally likely to be preceded by every

other trial type. Each run commenced and ended with a 12 s blank screen during which only the uniform gray background was shown to both eyes.

[Figure 1 about here]

Simultaneous with and independent of the grating stimuli, subjects performed a continuous foveal luminance change detection task, the timing of which was asynchronous with and independent of grating stimulus presentations. Throughout each run, a 0.2 degrees wide fixation cross was shown to both eyes in light green at the center of the display. Subjects were required to fixate the cross and respond to brief (0.2 s) decrements or increments in luminance of the central fixation cross by pressing one of two response buttons as quickly and accurately as possible. The magnitude of the luminance changes was varied in steps of 5% by a 1-up, 2-down staircase to maintain task difficulty approximately constant throughout the session. Luminance changes occurred at random intervals between 1 – 3 s long.

In a separate scanning session for each subject, standard phase-encoded retinotopic mapping procedures were used to identify and delineate cortical visual areas (Larsson and Heeger, 2006). For these experiments stimuli were displayed binocularly using a SANYO PLC XP40L LCD projector at 60 Hz and a resolution of 1024 x 768 pixels by backprojection onto a screen inside the bore of the scanner which subjects viewed through a front-silvered mirror. Retinotopic mapping stimuli consisted of dynamic black-and-white (100% contrast) radial checkerboard patterns displayed within wedge- or ring-shaped apertures that traversed the visual field with a period of 24 s (Larsson and Heeger, 2006). Wedge apertures extended between 0 and 13 degrees eccentricity and subtended 22.5 degrees polar angle; ring apertures were 0.75 deg wide in the radial dimension. The apertures moved stepwise by one aperture width every 1.5 s (synchronized with scanner data acquisition), such that apertures did not overlap but tiled the stimulated region of the visual field. For each aperture type, stimuli were run in both directions (clockwise/counter-clockwise and expanding/contracting) in separate runs. Between 1-4 runs of each direction were performed for each subject; each run consisted of 6 complete cycles of the stimulus. At the beginning and end of each run, a 24 s long blank screen was shown. Subjects performed the same luminance change detection task during retinotopic mapping scans as during the main experiment.

MRI acquisition

Visually evoked cortical blood oxygenation-level dependent (BOLD) fMRI responses were measured by T2*-weighted gradient-recalled echo (GRE) echoplanar imaging on a 3T whole-body MR scanner (Magnetom Trio; Siemens, Erlangen, Germany) equipped with a custom 8-channel posterior-head array coil (Stark Contrast, Erlangen, Germany). Functional MRI data were acquired from 19 oblique slices roughly parallel to the calcarine sulcus and covering the occipital and temporal cortex (interleaved slice acquisition, no gap between slices, voxel size 3 x 3 x 3 mm, TR=1500ms, TE=34ms, flip angle=85 deg). On each session, a whole-brain anatomical MR volume was acquired and used for spatial co-registration of data across sessions (voxel size 1 x 1 x 1 mm, MPRAGE sequence, TR=1830ms, TI=1100ms, TE=5.6ms, flip angle=11 deg). In a separate session, a high-resolution, high-contrast T1-weighted anatomical MR volume of each subject was acquired (voxel size 1 x 1 x 1 mm, MDEFT sequence (Deichmann, 2006), TR=7.9ms, TI=910ms, TE=2.5ms, flip angle=16 deg) and used for cortical surface reconstruction (Larsson, 2001).

fMRI data analysis

fMRI data from each run and session were motion corrected using the mcflirt software package (Jenkinson et al., 2002) and subsequently co-registered to each subject's high-resolution MR image using custom software (Nestares and Heeger, 2000), to allow visualization of data on cortical surfaces and co-registration of data across scanning sessions. For all analyses below, time series data were converted to percent signal change by dividing by the mean across time points and centering the data to zero mean, followed by high-pass filtering with a cut-off of 0.03 Hz.

Following preprocessing, fMRI data were analyzed as follows. First, visual areas V1-hV4 were delineated using conventional retinotopic mapping procedures described in detail previously (Larsson and Heeger, 2006). Separately for the wedge and ring stimulus runs, data from one of the two stimulus directions (counter-clockwise wedges and contracting rings, respectively) were time-reversed and averaged voxel-by-voxel with data from the other direction to cancel out hemodynamic response delays. Stimuli for the time-reversed runs were temporally shifted by 5 s to roughly align the evoked BOLD response time series for the forward and time-reversed runs. Each averaged data set was fit with a sinusoid of the retinotopic stimulus frequency to yield for each voxel a response

magnitude, phase, and coherence (correlation with best-fitting sinusoid at the stimulus frequency). Regions of interest (ROIs) corresponding to retinotopic visual areas V1-hV4 were identified on flattened cortical surface representations (flat maps) by visualizing the response phase for wedge and ring stimuli respectively (corresponding to polar angle and eccentricity). Visual area boundaries were manually identified on these flat maps by reversals in response phase to the wedge stimuli, using the cortical parcellation scheme described by Larsson and Heeger (2006).

Data from the main experiment were analyzed in two steps. First, an estimate of the stimulus-evoked BOLD response averaged across trials was computed for each visual area ROI (combined across hemispheres) by linear deconvolution (Burock and Dale, 2000) (Fig 1C). Second, this estimate was used to model the response to each of the 160 (4 orientations x 2 eyes x 20 repeats) individual trials, separately for each voxel. A separate regressor was constructed for each trial, consisting of a copy of the average stimulus-evoked response normalized to unit sum aligned with the onset of the trial, and zeros at all other time points. Regressors were centered on zero mean. Because of the long intertrial intervals regressors for individual trials were essentially uncorrelated ($r<0.15$). A general linear model, containing the set of regressors for all trials, was fit to the individual time series of each voxel, preprocessed as above. This yielded for each voxel a vector of beta values corresponding to the estimated BOLD response magnitude to each trial, and a coefficient of determination (R^2) representing the proportion of variance explained by the model. The vectors of response magnitudes for all voxels within each ROI were concatenated into a data matrix that was used as input for the multivariate classification analysis.

A complementary voxelwise analysis was performed to visualize patterns of orientation or eye preference in BOLD responses. For this analysis the average response to each of the eight trial types (4 orientations x 2 eyes) was computed using linear deconvolution (Burock and Dale, 2000). Linear contrasts were computed from these average responses comparing right versus left eye stimulation, 0 deg versus 90 deg orientation, and 45 deg versus 135 deg orientation. For each contrast, t-statistics were computed and visualized in visual field coordinates (estimated for each voxel from the retinotopic mapping scans), or on flattened cortical surface representations to identify large-scale patterns in orientation or eye preference.

Radial bias index

To assess the presence of a radial bias in orientation preference, we computed for each area a radial bias index *RI* as the Pearson correlation between the t-statistic for the linear contrast between orthogonal orientation pairs (0 vs 90 deg or 45 vs 135 deg) and a sinusoid varying with polar angle and having minima and maxima at the two orientations in the pair. This is equivalent to the correlation between the spatial distribution of voxelwise orientation preference (expressed as a t-statistic) across the visual field and a radial bias map with maxima and minima along the two orthogonal orientations. E.g., for the contrast between 0 and 90 deg orientations, the radial bias index was computed by correlating the t-values for every voxel with a sinusoidal function of the polar angle θ of each voxel with maxima at 0 and 180 deg, and minima at 90 and 270 deg (note the 90 degree [$\pi/2$] offset reflects the difference in origin between visual field coordinates and standard polar coordinates):

$$RI = Corr\left(t_i, \sin\left(\theta_i + \pi/2\right)\right) \quad (1)$$

For eye preference, we computed an index of nasotemporal bias by computing the mean t-statistic for the linear contrast between right and left eye stimulation, averaged across voxels within each hemifield, and comparing this metric across hemifields.

Multivariate pattern classification analysis

A linear support vector machine (SVM) algorithm was used to decode stimulus orientation or eye-of-origin respectively from the matrix of response magnitudes for each ROI. Classification was carried out using the publicly available LIBSVM software package .(Chang & Lin 2011). The same data was used to decode both orientation and eye-of-origin to allow a direct comparison of classification performance across stimulus categories. To equate the number of data samples per category for decoding orientation and eye-of-origin, data for oblique stimulus orientations (45 and 135 deg) and cardinal stimulus orientations (0 and 90 deg) were analyzed separately.

Only voxels exceeding a R^2 threshold of 0.35 were included in the classification (corresponding to on average 45 voxels per ROI in areas V1-V3). The relatively

conservative threshold ensured that only voxels showing a clear stimulus-evoked response were included in the classification and also resulted in the number of voxels always being smaller than the number of samples (trials). The specific threshold was chosen by trial and error to maximize classification performance across areas and stimuli. Lower or higher thresholds resulted in lower overall performance, but did not qualitatively change results. Similarly, the choice of parameters for the SVM procedure (specifically the soft margin parameter C) were chosen to maximize performance (using the built-in cross-validation function of LIBSVM), and we repeated the analyses with a range of parameters to ensure that other than overall lower decoding performance the results did not differ qualitatively with different parameters. To avoid biasing the analysis for a particular stimulus, parameter evaluation was done separately for cardinal and oblique orientations and for orientation and eye-of-origin respectively, and the parameters chosen that yielded the most similar performance across conditions.

Responses of voxels included in the classification analysis (i.e., voxels exceeding threshold) were normalized to unit vector length, so that mean responses across voxels did not differ between trials. This procedure ensured that any overall difference in response magnitude across all voxels (e.g. due to larger responses to one eye or orientation) could not drive decoding. The normalized voxel responses were subjected to a leave-one-out classification procedure, training the algorithm on data from four runs and testing decoding performance on the fifth, and repeating this with a different permutation of training and test data, so that data from every run was used for testing once. Decoding performance was assessed by the proportion of correctly classified trials. A bootstrap procedure (resampling with replacement) was used to compute confidence intervals for mean decoding performance, using 10,000 bootstrap iterations. Decoding performance was considered significantly better than chance if the lowest end of the 95% confidence interval of the bootstrapped means was above chance level performance. Significant differences in performance between decoding orientation and eye-of-origin, and between visual areas for each decoding type, were assessed by a non-parametric resampling test for each data permutation and subject. For this test, data for each subject and permutation were randomly assigned to one of two sets and the mean absolute difference in performance between the sets was computed. This procedure was repeated 10,000 times. The actual observed difference in performance was compared to the obtained resampled distribution and significance estimated as the proportion of resampled differences as large

as or larger than the observed value (two-tailed test).

To determine the spatial scale and structure of data driving decoding, we measured the effect of binning voxels according to several spatially organised parameters (e.g. polar angle and eccentricity) on decoding performance, compared to random (non-spatial) binning following the method of Freeman et al. (2011). Binning parameters for each voxel included in the classification were sorted and categorised into a variable number of bins containing equal numbers of voxels, and the response magnitudes of voxels within each bin averaged across trials prior to normalization. For each number of bins, we compared decoding performance using the binning parameter (e.g., eccentricity) with perfomance obtained by randomly assigning voxels to the same number of bins (ignoring any spatial structure in the data). Classification performance was measured for 11 numbers of bins in logarithmic steps from 1 to 1024. The largest number of bins exceeded the number of voxels, effectively meaning that every voxel was treated as a separate bin, and hence was equivalent to decoding without binning.

The effect of binning on decoding performance was quantified as the number of bins where decoding performance fell to one half of decoding performance without binning. First, decoding performance was rescaled to units of proportional reduction in error (PRE, also known as Klecka's tau τ), relative to chance level performance:

$$\tau = \frac{n_{corr} - \sum_{i=1}^{T} p_i n_i}{N - \sum_{i=1}^{T} p_i n_i} \qquad (2)$$

where n_{corr} is the number of correctly classified trials, n_i is the number of trials in the *ith* group, N is the total number of trials, T is the number of groups (2) and p_i is the probability of a trial being allocated to that group by chance ($p_i = 1 / T$). PRE values range from 0 (chance level) to 1 (corresponding to 100% correct performance). Decoding performance, expressed in units of PRE as a function of the number of bins, was then fit with a logistic function:

$$\tau = \frac{\tau_{max}}{1 + e^{-(x-n)/s}} \qquad (3)$$

where τ_{max} is decoding performance without binning, *n* is the number of bins at threshold performance ($\tau_{max}/2$), and *s* the slope of the function.

Resampling statistics were used to determine significant differences in classification performance (number of bins at threshold, *n*) between different types of binning. On each resampling iteration, the vector of classification performance as a function of bin size for each binning type, subject and permutation of test and training data was randomly assigned to one of two sets, and the slope *s* and threshold *n* estimated for each of the two sets by fitting equation (2) above. This procedure was repeated 10,000 times to yield a bootstrapped distribution of thresholds under the null hypothesis that the two types of binning did not differ in classification performance. Only thresholds from statistically significant fits (*F*-test, $P<0.05$) were included. The actual mean difference in thresholds between the two binning procedures was then compared to the bootstrapped distribution and significance estimated as the proportion of resampled threshold differences larger than or equal to the observed threshold differences (one-tailed test).

In a complementary analysis, we measured the impact of regressing out the effect of spatial parameters from the voxel data on decoding performance, analogous to the test of necessity used by Freeman et al. (2011). For this analysis each row (corresponding to a single trial) in the voxel data matrix used for classification was replaced with the residuals from fitting a linear regression model to the original data, using the spatial parameter as regressor, before running the classification analysis. By comparing the difference in decoding performance with and without regressing out the parameter of interest, we obtained a measure of the importance (or necessity) of that parameter for decoding. This procedure was repeated for a range of voxel R^2 thresholds from 0.3 to 0.7, and decoding performance (expressed as PRE values) was plotted as a function of voxel threshold. Analogous to the test for effect of binning, a logistic function was fit to each of the resulting plots for decoding with and without regressing out the parameter, and significant differences in decoding threshold estimated using a resampling test. This test was analoguous to that used to assess the effect of binning: on each of 10,000 resampling iterations, classification performance data for each subject, condition, and with or without

435 spatial bias regressed out was randomly assigned to two sets and a logistic function fit to
436 each resampled set. The actual mean difference in thresholds between the original data
437 and the data which had had angular position or hemifield regressed out procedures was
438 then compared to the resampled distribution and significance estimated as the proportion
439 of resampled threshold differences larger than or equal to the observed threshold
440 differences (one-tailed test).
441
442 *Effect of spatial filtering on classification performance*
443 As a complement to the binning analyses, we also investigated the effect of lowpass and
444 highpass spatial filtering of voxel responses on classification performance. To allow
445 comparison with previous studies we used similar procedures to those of Freeman et al
446 (2011) and Swisher et al. (2010). Voxel responses were lowpass filtered by iterative
447 weighted averaging with neighbouring voxels on the cortical surface, with weights
448 determined by intervertex distances using a Gaussian kernel (Chung et al., 2005; Larsson
449 2001). We empirically determined the number of iterations to obtain a specific filter width
450 for a given average intervertex distance (Hagler at al. 2006; Larsson 2001) and used these
451 estimates to lowpass filter the voxel responses with the following filter widths (FWHM): 2.2,
452 3, 5, 7, 9, 11, 13, 15, 17, 19, 21, 23, and 25 mm. Highpass filtered data were obtained by
453 subtracting the lowpass filtered data from the original unfiltered data. For each resulting
454 data set, we carried out the classification analysis and quantified decoding performance as
455 described above. Because the results were qualitatively similar for cardinal and oblique
456 orientations, decoding data for both sets of orientations were combined.
457
458 *Mapping perceptual eye dominance*
459 In a separate session for each subject, we measured the spatial distribution of eye
460 dominance across the visual field using a variation of a method based on binocular rivalry
461 (Handa et al., 2006; Yang et al., 2010) (Fig 1B). Circular patches containing 1 cpd gratings
462 tilted 45 deg left or right of vertical were shown dichoptically at each of 25 visual field
463 locations, with the two eyes shown orthogonal orientations. The 25 tested locations
464 included the fovea and 8 locations spaced evenly at 45 deg intervals starting from vertical
465 at each of three different eccentricities (1.5, 3 and 6 degrees from the fovea). To ensure
466 fixational stability subjects were required to fixate a central cross 1 deg wide displayed
467 binocularly. Patch size varied with eccentricity, being 1.125, 2.25, and 4.5 deg at the three
468 different stimulus eccentricities respectively. The foveal patch was 1.125 deg wide. Stimuli

were delivered using the same display system (NNL goggles) used for the fMRI experiments to ensure identical stimulus conditions. For each location, subjects pressed one of two keys continuously to report the perceived grating orientation (corresponding to the stimulus shown to one of the eyes), and the relative duration of exclusive stimulus visibility for each eye was recorded and used as an index of eye dominance at this location. Gratings were presented at 100% contrast (randomly changing phase at 10Hz) for 6 s at each location, and each location was tested twice in each run, with each of the two different stimulus orientations being shown to both eyes to cancel out any potential differences in orientation bias between the eyes. Trials were run back to back in random order. Five runs were performed for each subject, resulting in a total of ten measurements of eye dominance for each location, and the average relative perceived stimulus duration for each eye computed. A visual field map of perceptual eye dominance was constructed for each subject by linearly interpolating eye dominance across all visual field locations within 6 deg eccentricity.

Measuring correlations between maps

We computed the inter-area correlations between fMRI-based maps of orientation preference and eye dominance, as well as the correlation between maps of fMRI-based and perceptual eye dominance. For computing inter-area correlations, we interpolated V1 data to match the locations of corresponding voxels in V2 and V3 based on retinotopic location (polar angle and eccentricity). For computing correlations between fMRI-based eye dominance and perceptual eye dominance, the latter was interpolated to the visual field locations of voxels in each area. Because of spatial autocorrelations in these maps, conventional statistical estimates of correlation significance could not be used as these assume independence of measurements. Instead we used a resampling test known as the torus randomization procedure (Upton & Fingleton 1985; Fortin, & Payette 2002), which does not require assumptions about the underlying distribution or direct estimation of spatial autocorrelations. For each pair of maps, the procedure involves circularly shifting one of the maps by a given lag in each map dimension and computing the correlation between the shifted map and the other map. The significance of the correlation between the two maps is given by the proportion of computed correlations equal to or larger than the actual correlation between the (unshifted) maps. For the present study, the data were linearly interpolated onto a 50 x 50 grid. Each map was then shifted by one grid step at a time in each the two dimensions independently, yielding 2500 permutations. The

correlation between the maps was computed for each permutation and the distribution of correlations obtained used to estimate significance of the actual correlations. Because the procedure estimates significance as the proportion of correlations greater than or equal to the actual one, the resolution of the maps would not be expected to influence the results; however, to confirm this we also used a map resolution of 100 x 100, with similar results.

Results

Decoding performance for orientation and eye-of-origin

In all four visual areas examined, decoding perfomance was significantly above chance level both for orientation and eye-of-origin (Fig 1D). However, classification performance was significantly higher in V1-V3 than in hV4; in the latter area, decoding performance, although significant, was only marginally above chance level. For this reason only areas V1-V3 were included in subsequent analyses.

Classification performance did not differ significantly between decoding orientation and eye-of-origin in either area (resampling test, $P>0.1$). Moreover, performance did not differ between areas with the exception of V2, for which orientation decoding performance was significantly higher than in either V1 or V3 ($P<0.05$ and $P<0.01$ respectively, two-tailed resampling test), but only for oblique orientations.

If classification performance had reflected biased sampling of columnar-scale structures, we would have expected decoding performance for eye-of-origin to be much higher in V1 than extrastriate areas, as monocularly driven neurons have not been found beyond V1 in primate visual cortex (Hubel and Livingstone, 1987; Tootell and Hamilton, 1989) and anatomical (Adams et al. 2007), optical imaging (T'so et al. 1990) and fMRI (Nasr et al., 2016) studies all indicate that ocular dominance columns are confined to V1. Also, it might have predicted higher classification performance for decoding eye-of-origin than orientation, due to the differences in spatial organization of ocular dominance and orientation columns which, all else being equal, would predict larger voxel biases for eye preference than orientation, which in turn would be expected to translate into higher decoding performance. However, given the complex the relationship between spatial organization and decoding performance, which is influenced by many other factors, this prediction is not as clear-cut as it may appear. Note, however, that because we used the same data for both types of classification, we avoided the potentially confounding effect of

response strength on classification performance (Smith et al., 2011) that may have resulted from using different stimuli or experimental setups.

Our results did not conform to these predictions, as no significant differences in decoding performance were found between the two stimulus features, nor was classification performance for eye-of-origin higher in V1 than in extrastriate visual areas V2 and V3 (Fig. 2). Although the lack of significant differences in decoding performance for orientation and eye-of-origin failed to match predictions based on columnar organization in V1, this need not rule out a columnar origin of signals driving decoding in this area, given that decoding performance depends on many other parameters (Chaimow et al., 2011). However, the finding of significant decoding of eye-of-origin in V2 and V3 cannot be readily explained by a columnar origin of decoding signals, as ocular dominance columns have not been found beyond V1. These findings suggest that, at least for decoding eye-of-origin in V2 and V3, signals underlying classification are unlikely to derive from columnar-scale structures but may instead reflect larger-scale spatial variations in response bias.

Spatial scale of patterns underlying decoding

To determine the spatial scale of BOLD fMRI response patterns driving the classification, two complementary analyses were performed. First, large-scale retinotopic patterns in response biases were identified by visualizing voxel-wise stimulus preferences in visual field coordinates or on cortical flat maps (Figs 2 and 3). Second, we tested whether patterns of response biases were organized in a large-scale pattern by binning voxels according to their visual field location and assessing the effect on decoding performance (Freeman et al., 2011). If the pattern of response biases were correlated with visual field location, voxels with similar retinotopic location (eccentricity or polar angle) would have similar biases, and binning voxels by retinotopic location would not be expected to reduce decoding performance to the same degree as binning voxels randomly (which would tend to cancel out large-scale variations in response bias). Conversely, if response biases were due to local small-scale variations unrelated to retinotopic location, binning by retinotopy should confer no advantage for decoding compared to random binning, and both would be expected to reduce performance compared to decoding without binning.

Consistent with previous studies (Sasaki et al., 2006; Clifford et al., 2009; Freeman et al., 2011), orientation preference showed a clear and consistent radial bias, such that voxels

responded preferentially to the stimulus closest to a radial orientation (Fig 2A, B). Radial bias patterns in V2 and V3 were very similar to those in V1, but generally more pronounced, and this pattern was also consistent across subjects. We computed for each area an index quantifying the degree of radial bias (see Methods for details), which was significantly greater than expected by chance in 4/5 subjects in V1 and in every subject in V2 and V3 (F-test, P<0.01, FDR corrected for multiple comparisons) and was similar for both cardinal and oblique orientations (Fig 2C). Evidence of a radial bias could also be seen in the distribution of orientation preferences on the cortical surface (Fig 2D). For example, voxels in the ventral left hemisphere and dorsal right hemisphere parts of V1-V3 (corresponding to the visual field representations of the upper righthand and lower lefthand quadrants) show preference for 45 deg gratings over 135 degree gratings, whereas the remaining parts of V1-V3 show the opposite orientation preference, corresponding to the orientation closest to radial for each quadrant representation.

[Figure 2 about here]

Compared to orientation preference, the spatial pattern of eye preference was more variable between and within individuals (Fig 3B,C). Eye preference patterns were, however, strongly and significantly correlated between cardinal and oblique orientations (median r=0.56, range 0.24-0.91, P<0.001 in all areas), suggesting that eye preference is independent of orientation preference or stimulus orientation. This result also indicates that patterns of eye bias are stable within a session. In some subjects (e.g., S1, S3), a weak preference for the contralateral eye was evident in the visual field plots, consistent with nasotemporal asymmetries in eye preference found in macaque visual cortex (Horton and Hocking, 1996; Tychsen and Burkhalter, 1997) (Fig 3B,C). Notably, in agreement with our findings, Horton and Hocking (1996) also reported that this bias was modest and variable across individuals. A direct test of eye preference between voxels with left and right hemifield visual field location showed this hemifield bias to be significant in 4/5 subjects in V1 (resampling test of t-values for eye preference, P<0.05, FDR corrected for multiple comparisons), and in 3/5 subjects in V2 and V3, respectively. In some subjects (e.g. S4 and S5), eye preference also varied with eccentricity, with strong preference for one eye in the centre and weaker eye preference in the periphery. The weaker eye preference in the periphery may reflect the weaker responses elicited by the stimulus in voxels whose receptive fields only partially overlapped with the stimulus, rather than indicating a genuine

difference in eye preference between centre and periphery; a similar reduction in response bias at peripheral locations was also evident in plots of orientation preference (Fig 2). Although the pattern of eye preference varied across subjects, within each subject the pattern tended to be similar across visual areas V1-V3 (Fig. 3B). Surprisingly, given that monocularly driven neurons have only been found in V1, the magnitude of eye preference (as measured by the range of t-scores for right versus left eye stimulation) was similar between V1 and V2/V3, although in one subject (S5) magnitudes were larger in V1 (Fig. 3B).

The spatial distribution of eye preference shown in Fig. 3B rules out the possibility that poor binocular fusion of the fixation cross might have caused left and right eye stimuli to appear in different parts of the visual field. Had this been the case, it would have predicted the largest differences in eye preference along the left and right edges of the stimulus, with the left and right patterns being symmetrical but of opposite sign. Instead for the majority of subjects the strongest eye preferences were found in the central part of the visual field with little evidence of mirror-image symmetry along the outer left and right edges. We can also rule out the possibility that the patterns might simply have reflected non-uniform stimulation due to incomplete calibration of the goggle eye pieces, as this would have predicted a constant pattern in eye preference across subjects, rather than the subject-specific pattern evident in Fig 3B.

Hypothesizing that the pattern of eye preference measured by fMRI might correspond to spatial variations in eye dominance, in separate experiments we measured the retinotopic pattern of perceptual eye dominance in the same subjects within the central 6 deg of eccentricity corresponding to the stimulus size used in the fMRI experiments (Fig 3A). We conjectured that if the MRI-derived pattern in eye preference reflected neuronal ocular dominance, perceptual eye dominance should show a similar pattern across the visual field, based on previous fMRI studies showing that BOLD responses in V1 during binocular rivalry reflect the dominant percept in a spatially specific manner (Lee et al., 2005) and evidence suggesting stronger fMRI responses to dominant eye stimulation (Mendola and Conner, 2007). On the basis of these results, we predicted that the patterns of ocular dominance measured by fMRI should be associated with a corresponding spatial distribution of perceptual eye dominance. However, only for one subject (S1) was the pattern of perceptual eye dominance significantly correlated ($P<0.01$) with the pattern of

eye preference measured by fMRI in all three areas; in subject S3, perceptual eye dominance was also significantly correlated with fMRI eye preference but only in V3 (Fig 3B). Since fMRI and perceptual eye preference were measured on separate days, we cannot exclude the possibility that the two might be related, but fluctuate over long time scales; however, within each scanning session fMRI eye biases were stable, as evidenced by the correlation between eye preference patterns for oblique and cardinal orientations. Also, a different measure of perceptual eye dominance than the one used here (e.g. contrast sensitivity) might be more closely correlated with the patterns of fMRI eye preference.

[Figure 3 about here]

To determine whether the large-scale retinotopic patterns in the visual field maps (radial or hemifield/contralateral bias) could account for decoding orientation or eye-of-origin, we compared the effect on decoding performance of binning voxels by visual field location relative to random binning. If the pattern of fMRI responses were organized in a large-scale retinotopic fashion, we predicted that binning voxels by retinotopy should reduce decoding performance less than binning voxels randomly. Conversely, if response biases were due to random sampling of the underlying columnar structure, nearby voxels should show uncorrelated biases and binning by retinotopy should confer no benefit over random binning.

First, we examined the effect of binning voxels by polar angle on decoding performance (Fig 4A-C). Consistent with previous reports of a large-scale radial bias in orientation preference in early visual cortex (Sasaki et al., 2006; Clifford et al., 2009; Freeman et al., 2011), orientation decoding was significantly better when voxels were binned by polar angle than randomly both for cardinal and oblique orientations in V1 (resampling test, one-tailed, $P<0.001$ and $P<0.05$ respectively). In V2 and V3 the difference was significant only for oblique stimuli ($P<0.001$ and $P<0.01$, respectively). For oblique, but not cardinal, stimuli the effect was even more pronounced in V2 and V3 than in V1; in V3, decoding performance remained as high as 60% of the maximum performance (i.e., decoding performance without binning) with only four bins. The effect of binning by polar angle was consistent with the radial bias evident in the visual field plots and flat maps of orientation preference (Fig 2), as voxels with similar polar angle also had similar orientation

preference. These results confirm and extend the findings of Freeman et al (2011) suggesting that decoding of orientation relies largely on large-scale radial biases, as opposed to being due to random sampling of underlying columnar orientation patterns.

[Figure 4 about here]

Binning by polar angle did not, in general, improve performance for decoding eye-of-origin, compared to random binning (Fig 4D). Only in V2, and only for cardinal orientation stimuli, was decoding performance significantly better when binning by polar angle than random binning (resampling test, one-tailed, $P<0.05$). This result indicates that ocular dominance, as evident in BOLD fMRI responses, does not have a large scale organization in the polar angle dimension similar to that observed for orientation preference (although as reported above, eye dominance showed a weak hemifield bias in a majority of subjects).

A potential confound with binning by polar angle as a test of the importance of a large-scale spatial bias on classification, is that because nearby voxels have similar visual field locations, averaging voxels with similar polar angle tends to average nearby voxels, effectively being equivalent to local smoothing of voxel responses. If voxel orientation preferences were locally spatially correlated but did not show a large-scale radial bias, binning by polar angle might thus still be expected to be better than random binning simply because of such local correlations. To rule out this possibility we tested the effect of binning by eccentricity rather than polar angle on orientation decoding performance (Fig 4E-F). If the benefit of binning by polar angle had been due to averaging of nearby voxels rather than to a large-scale radial bias, then binning by eccentricity should also be better than random binning, as nearby voxels also have similar eccentricity. However, for decoding orientation, binning voxels by eccentricity had virtually no effect compared to random binning, showing only a slight improvement in V2 for cardinal orientations (resampling test, $P<0.05$). For decoding eye-of-origin, binning by eccentricity also did not improve decoding performance compared to random binning except for V3 for cardinal orientations only ($P<0.01$) and V1 for oblique orientations only ($P<0.05$). This may reflect the eccentricity variations in eye preference evident in some subjects (Fig 3, e.g. S5). Hence the effect of binning by polar angle on orientation decoding cannot be accounted for by locally correlated voxel responses, but reflects the radial bias in orientation preference.

To test whether the contralateral bias in eye preference found in a majority of subjects might account for decoding of eye-of-origin, we assessed the effect of binning by visual hemifield on decoding performance. Voxels were classified as being left or right hemifield based on their angular position (polar angle). Analogous to the analyses for polar angle and eccentricity, voxels were sorted into increasing numbers of equal-sized bins with all voxels within each bin (except one) being from a single hemifield (because the bins all contained the same number of voxels and the number of voxels in each hemifield was not an even multiple of the number of bins, one of the bins necessarily combined voxels across hemifields). For each bin, the responses of all voxels were replaced by the average response across voxels within the bin prior to running the classification analysis. The results indicated that a contralateral bias could indeed account for decoding eye-of-origin: in V1, binning by hemifield was associated with a strongly significant improvement in decoding performance ($P<0.01$ and $P<0.001$ for cardinal and oblique orientations respectively) (Fig 5D-F). In V2 and V3, the effect was smaller than in V1 but significant for at least one of the orientations in each area ($P<0.05$) (Fig 5D-F). The difference in results between binning by polar angle and binning by hemifield is consistent with a contralateral bias that is relatively uniform in the polar angle dimension within each hemifield. We also tested the effect of binning by hemifield on decoding orientation. Binning by hemifield was significantly ($P<0.05$ – $P<0.001$) better than random binning for decoding orientation (Fig 5A-C) in all areas (except V3 for cardinal orientations). This result is not directly predicted by radial bias in orientation preference, as the average radial bias in left and right hemifields should in principle cancel out. However, it may be explained by an imbalance in radial bias across the hemifields (e.g due to differences in the number or response magnitude of voxels with specific orientation biases). Alternatively, it could indicate the existence of a larger-scale bias for orientation distinct from radial bias, as previously suggested by Freeman et al (2013).

[Figure 5 about here]

The effect of binning by polar angle or hemifield on classification performance for orientation and eye-of-origin respectively demonstrated the existence of large-scale patterns in response biases that can drive decoding for these features. However it does

not rule out the possibility that response biases at other spatial scales can also contribute to decoding. To test whether the large-scale patterns were necessary for classification, we measured the effect of regressing out response biases correlated with angular position or hemifield on classification performance (Fig 6). At the voxel R^2 threshold used in the other tests (0.35), there was little effect of regressing out either feature, except in V2 for orientation decoding (Fig 6B). However, as R^2 threshold increased, orientation decoding performance dropped to chance level significantly faster when angular position had been regressed out of the voxel data in all three areas ($P<0.05$, $P<0.001$, and $P<0.01$ for V1-V3 respectively) (Fig 6 A-C). Similarly, for decoding eye-of-origin, there was a significant reduction in classification performance in V1 and V2 (but not V3) when the effect of hemifield had been regressed out. Therefore, although the binning tests above demonstrated that both large-scale patterns were *sufficient* for successful classification, these findings would suggest that only at high voxel thresholds were the patterns *necessary* for classification. This would indicate that information about both orientation and eye-of-origin is present at multiple spatial scales. However a more trivial possibility is that the regression procedure simply failed to remove the large-scale bias completely, allowing decoding to capitalize on residual effects. For example, we only regressed out a linear bias component from the voxel data; hence if the effect of the biases were not linearly proportional to the bias pattern, the non-linear component would have remained in the data. Although both interpretations are possible, given that Freeman et al. (2011) demonstrated the necessity of a radial bias (angular position) for decoding orientation, it seems more likely that our results reflect a failure to fully remove the large-scale bias component.

[Figure 6 about here]

If the original conjecture that patterns of eye preference measured by fMRI should reflect perceptual eye dominances had been correct, binning voxels according to perceptual eye dominance would also have been expected to improve decoding performance for eye-of-origin. However, as reported above, there was no consistent correlation between perceptual eye dominance and eye preference measured by fMRI across subjects. Nonetheless, we found that binning by perceptual eye dominance did in fact significantly improve decoding performance for eye-of-origin in all three visual areas (resampling test, $P<0.001$ and $P<0.05$ for V1 and V2/3 respectively).

We believe the most likely explanation for this somewhat surprising result is that because perceptual eye dominance was measured over a coarser spatial grid than fMRI responses, the resulting patterns were spatially smooth, meaning that binning voxels with similar perceptual eye bias was in effect equivalent to local averaging of nearby voxel responses (i.e. smoothing). Such smoothing would be expected to have less impact on decoding performance than completely random binning, if the patterns of voxel biases were also locally smooth (Shmuel et al., 2010).

To directly test this hypothesis, we compared the effect of binning by perceptual eye bias with binning voxels by the same bias patterns that had been reshuffled randomly across the 25 sampled visual field locations before being interpolated onto the voxel grid. The resulting reshuffled bias map had the same spatial smoothness as the measured map, but random large-scale pattern. Consistent with the hypothesis that the benefit of binning by perceptual eye dominance was due to the spatial smoothness of the perceptual dominance pattern, there was no significant difference in any of V1-V3 between binning by the measured pattern relative to the reshuffled pattern (resampling test, $P>0.1$). The only exception to this was for cardinal orientations in V1, where binning by reshuffled perceptual dominance resulted in a significant reduction in performance relative to binning by the unshuffled dominance patterns (resampling test, $P<0.05$).

To obtain a rough estimate of how the smoothness in perceptual eye dominance measurements translated to spatial scale in the cortex, we used estimates for cortical magnification and visual area sizes from Larsson and Heeger (2006). Perceptual eye dominance was sampled at a spacing of 45 degrees in the polar angle dimension, corresponding to a quarter of the width of V1. Assuming an average V1 width of 25 mm (Larsson and Heeger, 2006), this corresponds to a cortical spacing ~7mm, or 2-3 voxels; in the radial dimension the corresponding spacing was larger, approximately 15 mm (5 voxels) at 3 deg eccentricity (using the cortical magnification function for V1 in Larsson & Heeger (2006)). Because these distances are several voxels wide in both radial and polar dimensions, any local correlations in eye preferences are also likely to extend over a distance spanning multiple voxels and may reflect previously reported low frequency variations in eye preference observed at higher field strength (Shmuel et al., 2010).

Effect of spatial filtering on decoding performance

In a complementary analysis we measured the effect of spatially filtering voxel responses on decoding performance using methods comparable to those used in previous studies (Swisher et al. 2010, Freeman et al. 2011). For orientation decoding in V1, our results agree well with those of these previous studies. Lowpass filtering reduced decoding performance at larger filter widths, with a slight improvement at an intermediate filter width (5mm) consistent with fine-scale noise limiting classification for small or zero filter widths (Fig 7A). Highpass filtering resulted in a reduction of classification performance that was inversely proportional to filter width, relative to unfiltered data, with the largest reductions in performance at the smallest filter widths. For both types of filtering, the effects of filter width on decoding was significant (Spearman's rank order correlation, $P<0.01$ FDR corrected for multiple comparisons). These results are consistent with decoding relying on spatial biases at multiple scales but with the most information contained in larger scales. Swisher et al. (2010) and Freeman et al. (2011) did not measure decoding performance beyond V1, but our results for these areas were very similar to those of V1, especially in V2 (Fig 7B). Effects in V3 were less pronounced than in V1 and V2, but followed the same pattern (Fig 7C).

For eye-of-origin, the effects of spatial filtering were very similar to those observed for orientation, indicating that decoding relied on spatial biases primarily at intermediate and large spatial scales, with the smallest contribution from the smallest scales (Fig 7D-F). For lowpass filtered data, decoding performance decreased with increasing filter width for all but the smallest filter widths, suggesting the presence of small-scale noise in the data reducing decoding performance. Like for orientation, the effects in V2 were very similar to those in V1 (Fig 7E), but somewhat less pronounced in V3; specifically, for highpass filtered data there was no significant correlation between filter width and decoding performance in V3 ($P>0.1$) (Fig 7F).

[Figure 7 about here]

Origin of response biases in extrastriate cortex

The similar effects of spatial filtering on decoding orientation and eye-of-origin suggests that the spatial biases of both features are similar in scale; notably, for both features the evidence suggests most information is contained at larger spatial scales. Moreover, the

similarity between the effects in V1 and extrastriate areas V2 and V3 also suggest the scale of spatial biases are similar across areas. These results are consistent with the finding that decoding performance both for orientation and eye-of-origin was as high in V2 and V3 as in V1, and similar for both features. However, neither of these observations is well predicted by random sampling of columnar-scale patterns of orientation or eye preference underlying decoding. In particular, the lack of difference between V1 and V2/V3 for decoding eye-of-origin is not consistent with a columnar origin, given that ocular dominance columns (or indeed monocularly driven neurons) have not been observed beyond V1 (Hubel and Livingstone, 1987; Tootell and Hamilton, 1989). We conjectured that the pattern of response biases in V2 and V3 might instead originate in V1 and be propagated to these areas through the topographic projections from V1 to extrastriate areas. Because of the topographic organization of V1-V3, large-scale patterns of eye preference in extrastriate areas would be expected to be spatially correlated with V1 eye preference patterns. Moreover, binning voxels by the pattern of V1 eye preference should improve decoding performance in V2 and V3 relative to random binning. The results of testing these two predictions are shown in Figure 8.

[Figure 8 about here]

Both for orientation and eye preference, the patterns of preferences in V2 and V3 were significantly correlated with the corresponding patterns in V1, both across ($P<0.001$; Fig 8A-B) and within (torus randomization test, $P<0.05$; Fig 8C) subjects. Eye preferences in V2 and V3 had lower magnitude than in V1, as might be expected if the patterns of eye preferences in these areas were largely reflecting V1 afferent synaptic input, rather than neuronal (spiking) output activity. Consistent with these correlations, binning by V1 eye or orientation preference significantly improved decoding performance for eye-of-origin and orientation, respectively ($P<0.01$ – $P<0.001$; Fig 8D-F). For decoding eye-of-origin, the effect was only significant for cardinal orientations; for orientation it was significant for both cardinal and oblique stimuli. It should be emphasized that correlation with the V1 pattern of preference is a conservative measure that likely underestimates the influence of inherited input, as the divergence of projections from V1 to extrastriate areas means that the pattern of input from V1 to higher areas is unlikely to be a simple replication of the pattern of V1 activity.

In summary, our results demonstrate that both orientation preference and ocular dominance show evidence of large- or intermediate-scale patterns in voxel biases that contribute to decoding these features from fMRI data. For decoding orientation, this pattern primarily reflects the radial bias in orientation preference reported in previous studies. For decoding eye-of-origin, we found that the pattern reflected a contralateral bias in eye preference previously observed only by single-unit recordings (Horton and Hocking, 1996; Tychsen and Burkhalter, 1997). For both types of classification, there was evidence consistent with decoding in extrastriate areas being driven at least in part by large-scale spatial response biases originating in V1.

Discussion

The results of this study replicate previous reports of large-scale biases driving multivariate classification analysis of orientation representation in early visual cortex, and extend these findings by identifying a similar bias for ocular dominance. Consistent with previous studies (Sasaki et al., 2006; Clifford et al., 2009; Freeman et al., 2011, 2013), we found a large-scale radial bias for orientation that could largely account for decoding of orientation in V1-V3. A novel finding of this study is that decoding of eye-of-origin can be explained by a large-scale (hemifield) bias for the contralateral eye. Whereas anatomical studies in non-human primates have found evidence for nasotemporal differences in eye preference (Horton and Hocking, 1996; Tychsen and Burkhalter, 1997), it has not been previously demonstrated in human visual cortex, nor has it been shown that such a bias can account for classification of eye-of-origin, although the possibility that a nasotemporal bias might drive classification was suggested by Shmuel et al (2010). We also found evidence that the pattern of eye bias in the BOLD response was locally smooth (evidenced by the improved decoding performance when binning by reshuffled eye dominance patterns), confirming previous studies at higher field strength (Shmuel et al., 2010). These results indicate that decoding eye-of-origin can rely on response biases at multiple spatial scales. The existence of biases at multiple scales is also supported by our finding that decoding was still possible, though performance was impaired, when the effect of hemifield had been regressed out of the data. Notably, however, none of these patterns are well explained by random sampling of an underlying columnar-scale pattern (which would be spatially uncorrelated, especially at large scales); instead they may rather reflect low

spatial frequency variations in eye preference in V1 demonstrated by quantitative measurements of ocular dominance column area in human and non-human primates (Horton and Hocking, 1996; Adams et al., 2007). This explanation cannot, however, account for the high decoding performance in V2 and V3 as these areas lack ocular dominance columns. The biases driving decoding in these areas must therefore reflect larger scale patterns of eye preference in neuronal responses in extrastriate areas, which have not been previously reported in neuronal recordings from these areas in non-human primates. Our finding of large-scale biases in eye preference also argues against the idea that these biases are induced by stimulus properties, as has been suggested for orientation stimuli (Alink et al., 2013; Carlson 2014). Whether these biases have any perceptual correlates remains unclear; although we found no consistent correlation between the patterns of eye preference measured by fMRI and behaviourally, because these were measured on separate days, we cannot rule out the possibility that the two are linked but co-vary over longer time scales. The large-scale nasotemporal bias in eye preference is however likely to be fixed, given that it has also been found in anatomical studies (Horton and Hocking, 1996; Tychsen and Burkhalter, 1997). We measured perceptual eye preference in terms of relative duration of the dominant percept under binocular rivalry conditions; it is possible that a different metric, such as spatial variations in contrast sensitivity of each eye, might be more closely related to the variations in fMRI eye preference.

In contrast with Freeman et al. (2011), we found that regressing out the effects of angular position and hemifield reduced, but did not entirely abolish decoding performance, with classification remaining above chance level except at very high voxel thresholds. This could be interpreted as evidence that information about orientation and eye-of-origin exists at multiple spatial scales, as suggested above, but this idea is difficult to reconcile with the results of Freeman et al. (2011) who found that decoding was reduced to chance level when the effect of angular position was removed from the data prior to classification. The discrepancy in results might reflect differences in stimulus protocol – our study used an event-related design, with only four orientations, whereas Freeman et al. (2011) used a periodic stimulus design with 16 different orientations. It is possible that the transient responses in the event-related design we used contain orientation-tuned information at different (and smaller) spatial scales to that in the sustained response measured by a slowly varying periodic stimulus, as suggested by a recent study (Pratte et al. 2016). We

also used SVM (which is widely used in decoding studies) rather than linear discriminant analysis and only classified between two orientations for any given analysis, as opposed to the sixteen used by Freeman et al. (2011), which together may have helped make our analysis more robust to removal of the main source of orientation bias. An alternative (not mutually exclusive) interpretation is that we were unable to regress out completely the effects of angular position or hemifield. Because we used only two orientations for any individual classification (and, obviously there were only two eyes), we could not use the method by Freeman et al. (2011) to regress out a separate stimulus vector independently from every voxel, as this would have meant regressing out an effect that was perfectly correlated with the stimulus design and would thus trivially have removed any biases in the data. Instead we removed a constant pattern across voxels separately for each trial, which may have been less effective at removing variations across voxels. It is also possible (indeed likely) that the effect of large-scale biases is not linear, such that a complete removal of the effects would have required fitting a more complex model (i.e. including some non-linear transformation of angular position or hemifield).

While our results do not speak directly to whether the biases driving decoding eye-of-origin reflect actual neuronal response selectivities or vascular biases (Gardner, 2010; Shmuel et al., 2010), a purely vascular origin seems unlikely given that low-frequency spatial variations in eye preference have been found using metabolic measurements that do not depend on vasculature (Adams et al., 2007). Also, the correlations in eye preference patterns between V1 and extrastriate areas argue against a vascular origin of decoding signals, as a purely vascular bias would not be expected to be correlated across areas.

How well does decoding performance reflect neuronal response properties?

Several aspects of our results have implications for the interpretation of multivariate classification analysis of BOLD fMRI data. First, because classification performance depends both on the spatial distribution of voxel biases and the relative strength of those biases (Chaimow et al., 2011; Smith et al., 2011; Tong et al., 2012), it is unclear to what extent decoding performance reflects the underlying neuronal response properties of a cortical region. Our results suggest that at least for early visual areas and one of the stimulus features, ocular dominance, decoding performance is not well predicted by what is known about the neuronal response properties of these areas. Whereas monocular neurons are common in input layers of V1, where they are organized into well-defined

ocular dominance columns both in macaque (LeVay et al., 1985) and human visual cortex (Adams et al., 2007) there is little evidence of either monocularly driven neurons or spatial variations in ocular dominance in extrastriate visual areas (Hubel and Livingstone, 1987; Tootell and Hamilton, 1989; T'so et al. 1990; Nasr et al., 2016). This distribution of response properties would predict that decoding performance for eye-of-origin should be high in V1, and low in extrastriate areas, yet we found that decoding performance for eye-of-origin was not significantly lower in either V2 or V3 than in V1 (Fig 2). It is of course possible that this observation reflects a true interspecies difference, with human extrastriate cortex containing a greater proportion of neurons with strong eye preferences than its non-human primate counterpart. Alternatively, the discrepancy might reflect differences in methodology, as eye preference in non-human primates has largely been measured using spiking activity or metabolic rate rather than BOLD fMRI. Evidence suggests that BOLD signals may more strongly reflect synaptic input than output spiking activity (Logothetis, 2002). Hence, if the patterns of response biases in V2 and V3 were largely driven by spatially varying afferent input from V1 which was not reflected in the spiking output of these areas, this would explain the mismatch between our results suggesting strong ocular biases in extrastriate areas and physiological studies showing little or no evidence of eye preference in neuronal spiking responses in these areas. A third, not mutually exclusive interpretation, is that the biases might also be present in spiking output, but too weak and varying over such large spatial scales as to not be evident in the typically relatively localized recordings from comparatively small numbers of neurons in physiological studies. Without directly comparable measurements of eye preference in human and non-human primate cortex, it is difficult to rule out either of these possibilities. Nonetheless, the discrepancy between MVPA and single-unit physiology suggests that decoding performance of eye-of-origin cannot be straightforwardly predicted by known underlying variations in eye preferences of single neurons. We have previously reported a similar mismatch between MVPA and predictions based on direct neuronal recordings for decoding of luminance in human visual cortex (Hammett et al., 2013). For orientation selectivity, however, decoding performance at least qualitatively agreed with predictions based on the known physiological properties of early visual areas. High proportions of orientation-selective neurons have been found in all of V1-V3, (De Valois et al., 1982; Levitt et al., 1994; Gegenfurtner et al., 1996, 1997), predicting that decoding performance should be similar in the three areas, consistent with our results (Fig 1D). We emphasize that this qualitative correspondence between decoding and predictions based

on neuronal response properties does not imply that the MVPA results should be interpreted as quantitative measures of the underlying orientation tuning of individual neurons in these areas; simply that unlike the case for ocular dominance, decoding results for orientation are not directly at odds with the known physiology of visual cortex in non-human primates.

Our results thus suggest that interpreting decoding performance as a straightforward measure of neuronal response properties is non-trivial and can be potentially misleading. For the stimuli used in this study, we have the benefit of extensive prior knowledge about the response properties of early visual areas obtained by direct neuronal recordings in non-human primates, which allow us to determine how well decoding performance compares to the underlying neuronal response properties. For studies using more complex stimuli investigating higher visual areas for which the corresponding non-human primate homologues are either not known, and/or electrophysiological data is much more limited, such a comparison may be difficult or even impossible. The interpretation of decoding performance is further complicated by evidence suggesting that part of the biases driving decoding could reflect vascular drainage patterns (Gardner, 2010; Shmuel et al., 2010) which might be only indirectly related to the pattern of neuronal response biases. Needless to say, many of these issues derive from the relatively coarse spatial resolution used here and in most decoding studies; some of these concerns might be addressed by fMRI measurements at very high (columnar-scale) spatial resolution. However, the formidable technical challenges of such measurements (and the limited availability of high-field scanners) mean that for the foreseeable future the majority of decoding studies will continue to use conventional spatial resolutions, and hence be subject to the limitations highlighted by the conclusions of this study.

In summary, the results of this study add to a growing body of evidence suggesting that the results of multivariate pattern classification analysis of fMRI data need to be interpreted with caution, in particular when used to quantify functional properties of cortical areas, or to map the distribution of response tuning across the cortex in a comparative fashion. Indeed, these techniques may instead be best suited to address questions that do not rely on a direct correspondence between decoding performance and neuronal response selectivities, for example using MVPA as a biomarker or diagnostic tool (Brodersen et al., 2012). Furthermore, if the key response properties of the areas under investigation are

sufficiently well known (e.g., orientation selectivity in V1), the high sensitivity of multivariate classification methods (relative to univariate techniques) make these methods well suited to characterising distributed neural representations (Brouwer and Heeger, 2009) and investigating how such representations interact or are modulated by cognitive or experimental manipulations (Kamitani and Tong, 2006; Brouwer and Heeger, 2011; Hammett et al., 2013; Merriam et al., 2013).

Grants

This work was supported by Wellcome Trust grant WT090749MA to JL.

References

Adams DL, Sincich LC, Horton JC (2007) Complete pattern of ocular dominance columns in human primary visual cortex. J Neurosci 27:10391–10403.

Alink A, Krugliak A, Walther A, Kriegeskorte N (2013) fMRI orientation decoding in V1 does not require global maps or globally coherent orientation stimuli. Frontiers Psych, 4:1:14.

Bartels A, Logothetis NK, Moutoussis K (2008) fMRI and its interpretations: an illustration on directional selectivity in area V5/MT. Trends Neurosci 31:444–453.

Beckett A, Peirce JW, Sanchez-Panchuelo R-M, Francis S, Schluppeck D (2012) Contribution of large scale biases in decoding of direction-of-motion from high-resolution fMRI data in human early visual cortex. Neuroimage 63:1623–1632.

Blasdel GG (1992) Orientation selectivity, preference, and continuity in monkey cerebral cortex. J Neurosci 12:3139-3161.

Brodersen KH, Wiech K, Lomakina EI, Lin C-S, Buhmann JM, Bingel U, Ploner M, Stephan KE, Tracey I (2012) Decoding the perception of pain from fMRI using multivariate pattern analysis. Neuroimage 63:1162–1170.

Brouwer GJ, Heeger DJ (2009) Decoding and reconstructing color from responses in human visual cortex. J Neurosci 29:13992–14003.

Brouwer GJ, Heeger DJ (2011) Cross-orientation suppression in human visual cortex. J Neurophysiol 106:2108–2119.

Burock MA, Dale AM (2000) Estimation and detection of event-related fMRI signals with temporally correlated noise: a statistically efficient and unbiased approach. Hum Brain Mapp 11:249–260.

Carlson, TA (2014) Orientation decoding in human visual cortex: new insights from an unbiased perspective. J Neurosci 34:8373-8383.

Chaimow D, Yacoub E, Ugurbil K, Shmuel A (2011) Modeling and analysis of mechanisms underlying fMRI-based decoding of information conveyed in cortical columns. Neuroimage 56:627–642.

Chang C-C., Lin, C-J. (2011) LIBSVM: a library for support vector machines. Acm Trans Intell Syst Technol 2:1–27.

Cheng K, Waggoner RA, Tanaka K (2001) Human ocular dominance columns as revealed by high-field functional magnetic resonance imaging. Neuron 32:359–374.

Chung MK, Robbins SM, Dalton KM, Davidson RJ, Alexander AL, Evans AC (2005). Cortical thickness analysis in autism with heat kernel smoothing. Neuroimage 25(4):1256-65.

Clifford CWG, Mannion DJ, McDonald JS (2009) Radial biases in the processing of motion and motion-defined contours by human visual cortex. J Neurophysiol 102:2974–2981.

Deichmann R (2006) Fast structural brain imaging using an MDEFT sequence with a FLASH-EPI hybrid readout. Neuroimage 33:1066–1071.

De Valois RL, Yund EW, Hepler N (1982) The orientation and direction selectivity of cells in macaque visual cortex. Vision Res 22:531–544.

Fortin, M-J., Payette, S. (2002) How to test the significance of the relation between spatially autocorrelated data at the landscape scale: A case study using fire and forest maps. EcoScience 9:213–218.

Freeman J, Brouwer GJ, Heeger DJ, Merriam EP (2011) Orientation decoding depends on maps, not columns. J Neurosci 31:4792–4804.

Freeman J, Heeger DJ, Merriam EP (2013). Coarse-scale biases for spirals and orientation in human visual cortex. J Neurosci. 33(50):19695-703.

Gardner JL (2010) Is cortical vasculature functionally organized? Neuroimage 49:1953–1956.

Gegenfurtner KR, Kiper DC, Fenstemaker SB (1996) Processing of color, form, and motion in macaque area V2. Vis Neurosci 13:161–172.

Gegenfurtner KR, Kiper DC, Levitt JB (1997) Functional properties of neurons in macaque area V3. J Neurophysiol 77:1906–1923.

Hagler DJ Jr, Saygin AP, Sereno MI (2005) Smoothing and cluster thresholding for cortical surface-based group analysis of fMRI data. Neuroimage. 33(4):1093-103

Hammett ST, Smith AT, Wall MB, Larsson J (2013) Implicit representation of luminance and the temporal structure of motion in human visual cortex revealed by multivariate pattern classification analysis. J Neurophysiol.110:688-99.

Handa T, Uozato H, Higa R, Nitta M, Kawamorita T, Ishikawa H, Shoji N, Shimizu K (2006) Quantitative measurement of ocular dominance using binocular rivalry induced by retinometers. J Cataract Refract Surg 32:831–836.

Haxby JV, Gobbini MI, Furey ML, Ishai A, Schouten JL, Pietrini P (2001) Distributed and overlapping representations of faces and objects in ventral temporal cortex. Science 293:2425–2430.

Haynes J-D, Rees G (2005) Predicting the orientation of invisible stimuli from activity in human primary visual cortex. Nat Neurosci 8:686–691.

Horton JC, Hocking DR (1996) Intrinsic variability of ocular dominance column periodicity

in normal macaque monkeys. J Neurosci 16:7228–7239.

Hubel DH, Livingstone MS (1987) Segregation of form, color, and stereopsis in primate area 18. J Neurosci 7:3378–3415.

Jenkinson M, Bannister P, Brady M, Smith S (2002) Improved optimization for the robust and accurate linear registration and motion correction of brain images. Neuroimage 17:825–841.

Kamitani Y, Sawahata Y (2010) Spatial smoothing hurts localization but not information: pitfalls for brain mappers. Neuroimage 49:1949–1952.

Kamitani Y, Tong F (2005) Decoding the visual and subjective contents of the human brain. Nat Neurosci 8:679–685.

Kamitani Y, Tong F (2006) Decoding seen and attended motion directions from activity in the human visual cortex. Curr Biol 16:1096–1102.

Kanal E, Borgstede JP, Barkovich AJ, Bell C, Bradley WG, Felmlee JP, Froelich JW, Kaminski EM, Keeler EK, Lester JW, Scoumis EA, Zaremba LA, Zinninger MD, American College of Radiology (2002) American College of Radiology White Paper on MR Safety. Ajr Am J Roentgenol 178:1335–1347.

Krekelberg B, Boynton GM, van Wezel RJA (2006) Adaptation: from single cells to BOLD signals. Trends Neurosci 29:250–256.

Larsson J (2001) Imaging vision: functional mapping of intermediate visual processes in man. PhD Thesis, Karolinska institutet, Stockholm. ISBN: 91-7349-090-3

Larsson J, Heeger DJ (2006) Two retinotopic visual areas in human lateral occipital cortex. J Neurosci 26:13128–13142.

Logothetis NK (2002) The neural basis of the blood-oxygen-level-dependent functional magnetic resonance imaging signal. Philos Trans R Soc Lond B Biol Sci. 357:1003-37.

Lee S-H, Blake R, Heeger DJ (2005) Traveling waves of activity in primary visual cortex during binocular rivalry. Nat Neurosci 8:22–23.

LeVay S, Connolly M, Houde J, Van Essen DC (1985) The complete pattern of ocular dominance stripes in the striate cortex and visual field of the macaque monkey. J Neurosci 5:486–501.

Levitt JB, Kiper DC, Movshon JA (1994) Receptive fields and functional architecture of macaque V2. J Neurophysiol 71:2517–2542.

Mendola JD, Conner IP (2007) Eye dominance predicts fMRI signals in human retinotopic cortex. Neurosci Lett 414:30–34.

Merriam EP, Gardner JL, Movshon JA, Heeger DJ (2013) Modulation of visual responses by gaze direction in human visual cortex. J Neurosci 33:9879–9889.

Nasr S, Polimeni JR, Tootell RBH (2016) Interdigitated color- and disparity-selective columns within human visual cortical areas V2 and V3. J Neurosci 36: 1841-1857

Nestares O, Heeger DJ (2000) Robust multiresolution alignment of MRI brain volumes. Magn Reson Med 43:705–715.

Obermayer K, Blasdel GG (1993) Geometry of orientation and ocular dominance columnes in monkey striate cortex. J Neurosci 13:4114-4129.

Op de Beeck HP (2010) Against hyperacuity in brain reading: spatial smoothing does not hurt multivariate fMRI analyses? Neuroimage 49:1943–1948.

Sasaki Y, Rajimehr R, Kim BW, Ekstrom LB, Vanduffel W, Tootell RBH (2006) The radial bias: a different slant on visual orientation sensitivity in human and nonhuman primates. Neuron 51:661–670.

Sawamura H, Orban GA, Vogels R (2006) Selectivity of neuronal adaptation does not match response selectivity: a single-cell study of the FMRI adaptation paradigm. Neuron 49:307–318.

Schwarzkopf DS, Schindler A, Rees G (2010) Knowing with which eye we see: utrocular discrimination and eye-specific signals in human visual cortex. PLOSOne 5:e13775.

Shmuel A, Chaimow D, Raddatz G, Ugurbil K, Yacoub E (2010) Mechanisms underlying decoding at 7 T: Ocular dominance columns, broad structures, and macroscopic blood vessels in V1 convey information on the stimulated eye. NeuroImage 49:1957–1964.

Smith AT, Kosillo P, Williams AL (2011) The confounding effect of response amplitude on MVPA performance measures. Neuroimage 56:525–530.

Swisher JD, Gatenby JC, Gore JC, Wolfe BA, Moon C-H, Kim S-G, Tong F (2010) Multiscale pattern analysis of orientation-selective activity in the primary visual cortex. J Neurosci 30:325–330.

Tong F, Harrison SA, Dewey JA, Kamitani Y (2012) Relationship between BOLD amplitude and pattern classification of orientation-selective activity in the human visual cortex. Neuroimage 63:1212–1222.

Pratte MS, Sy JL, Swisher JD, Tong F (2016) Radial bias is not necessary for orientation decoding. Neuroimage. 127:23-33.

Tootell RB, Hamilton SL (1989) Functional anatomy of the second visual area (V2) in the macaque. J Neurosci 9:2620–2644.

Ts'o DY, Frostig RD, Lieke EE, Grinvald A (1990) Functional organization of primate visual cortex revealed by high resolution optical imaging. Science 249:417-20.

Tychsen L, Burkhalter A (1997) Nasotemporal asymmetries in V1: Ocular dominance columns of infant, adult, and strabismic macaque monkeys. J Comp Neurol 388:32–46.

Upton, G.J.G, Fingleton, B. (1985) Spatial Data Analysis by Example. Volume 1: Point Pattern and Quantitative Data. New York: J. Wiley & Sons.

Yacoub E, Harel N, Ugurbil K (2008) High-field fMRI unveils orientation columns in humans. Proc Natl Acad Sci U S A 105:10607–10612.

Yacoub E, Shmuel A, Logothetis N, Uğurbil K (2007) Robust detection of ocular dominance columns in humans using Hahn Spin Echo BOLD functional MRI at 7 Tesla. Neuroimage 37:1161–1177.

Yang E, Blake R, McDonald JE 2nd (2010) A new interocular suppression technique for measuring sensory eye dominance. Invest Ophthalmol Vis Sci 51:588–593.

Figure legends

Figure 1. Experimental design and analysis.
A. Event-related fMRI design (single trial shown). Stimulus images consisted of 1 cpd sinusoidal luminance gratings shown within an annular aperture against a uniform gray background. On each trial, sinusoidal gratings of a single orientation were displayed monoptically for 6s (the other eye shown a blank gray background). The spatial phase of the gratings changed randomly every 100ms. Trials were separated by intervals (gray background) varying randomly in length between 12s-24s. Subjects performed a luminance change detection task on a central fixation cross shown dichoptically.
B. Measurement of perceptual eye dominance (two consecutive trials shown). Stimuli consisted of 1 cpd sinusoidal luminance gratings oriented 45 left or right of vertical, displayed within circular patches at each of 25 locations across the visual field. On each 6s trial, a grating stimulus patch was shown for duration of the trial at one location, the two eyes being shown orthogonal orientations (randomly chosen). Subjects continuously pressed one of two keys to indicate the perceived orientation of the stimulus. Eye preference at each location was computed as the fraction of time dominated by the right eye stimulus.
C. Time course of stimulus-evoked BOLD response for individual subjects. Each time series shows the stimulus-evoked response (averaged across stimulus conditions and ROIs) estimated by linear deconvolution and averaged across visual areas V1-hV4. Error bars, average standard error of the estimate (square root of average error variance across ROIs) for each time point.
D. Classification performance for orientation and eye-of-origin in visual areas V1-hV4. Height of bars indicates proportion of correctly classified trials for each stimulus type. In areas V1-V3, classification performance is significantly above chance level (dotted line) both for orientation and eye of origin for both stimulus orientations; in hV4, classification performance is only significant for oblique stimuli. Error bars, standard error of the mean across subjects.

Figure 2. Spatial distribution of orientation preference measured by fMRI.
A. Spatial distribution of orientation preference plotted in visual field coordinates for each voxel for areas V1-V3 across all subjects. Each plot symbol corresponds to a single voxel, with color representing t-value indicating relative preference for horizontal (0 deg) versus

vertical (90 deg) stimuli (inset color map). The size of each plot symbol indicates goodness-of-fit (R^2) of voxel time series. Dotted circles show location of inner and outer boundaries of stimuli in visual field coordinates. For each area, preference for horizontal orientations predominates along the horizontal meridian whereas preference for vertical orientations is found mainly along the vertical meridian, consistent with bias for radial orientations.

B. Same as (A) but for oblique orientation stimuli. Color represents t-value indicating relative preference for rightward oblique (45 deg) versus leftward oblique (135 deg) orientation. Orientation preference shows a radial bias with voxels preferring 45 deg orientation having receptive fields (RFs) centered on the upper righthand and lower lefthand quadrants, whereas voxels preferring the orthogonal orientation have RF centers in the other two quadrants.

C. Radial bias index for areas V1-V3 for cardinal and oblique stimuli. Radial bias is defined as the correlation between the spatial distribution of orientation preference (panels A and B) and the radial bias map for each pair of orientations (polar sinusoid pattern shown in inset circular color maps in panels A and B) (see Methods for details). In all three areas, the average radial bias index was significantly greater than predicted by chance (t-test, $P<0.02$, FDR corrected for multiple comparisons). Error bars, standard error of the mean across subjects.

D. Cortical flat maps from the left and right hemisphere of a representative subject (S2) showing the distribution of relative orientation preference for oblique orientation stimuli in visual cortical areas V1-hV4. Color code as in (B). Voxels preferring rightward oblique orientation (45 deg) predominate in the lower hemifield representations of V1-V3 in the right hemisphere and upper hemifield representations in the left hemisphere, corresponding to the spatial distribution of orientation preference shown in (B); voxels preferring the orthogonal orientation predominate in the other two quadrants.

Figure 3. Spatial distribution of eye preference measured behaviourally and by fMRI.

A. Spatial distribution of perceptual eye dominance within 6 deg eccentricity for each subject. Color indicates relative preference for right or left eye stimulation (measured at 25 different visual field locations as the proportion of stimulus duration dominated by the corresponding eye; see Methods for details). Dotted lines indicate inner and outer boundaries of stimuli used in fMRI experiments.

B. Spatial distribution of eye preference measured by fMRI for areas V1-V3 for each

subject. Color represents t-values indicating relative preference for right versus left eye stimulation (inset t-map) for each voxel; size of plot symbols indicate goodness-of-fit (R^2) of linear model fit to each voxel time series. Dotted lines indicate inner and outer boundaries of stimuli. Numbers and asterisks next to each plot indicate strength and significance of correlation with perceptual eye dominance in (A) (see text for details). *, P<0.05; **, P<0.01; ***, P<0.001.

C. Nasotemporal eye preference in V1-V3. Height of bars shows average eye preference across subjects (t-value of contrast between right and left eye stimulation averaged across orientations) for right hemifield (RH, black bars) and left hemifield (LH, white bars) voxels (corresponding to left and right hemispheres, respectively). Numbers to the right of each plot indicate proportion of subjects showing significant contralateral preference (resampling test, P<0.05, FDR corrected for multiple comparisons). Error bars, standard error of the mean across subjects.

Figure 4. Effect of binning by visual polar angle and eccentricity on classification performance for decoding orientation and eye-of-origin in areas V1-V3.

A. Classification performance (proportion reduction in error) for decoding cardinal stimulus orientation (0 or 90 deg) in area V1 as a function of number of bins. *Filled symbols:* Binning voxels by polar angle. *Open symbols:* Binning voxels randomly. Decoding performance is significantly higher for binning by polar angle than random binning, consistent with a radial bias in orientation preference. Error bars standard error of the mean across subjects.

B-C. Threshold performance ($\log_2$ number of bins) for decoding orientation in V1-V3 for cardinal and oblique orientation stimuli for binning by polar angle (filled bars) and random binning (open bars). Decoding performance is significantly higher for binning by polar angle than random binning in all three areas (in V2 and V3 for oblique orientations only), as predicted by radial bias for orientation in these areas. *, P<0.05; **, P<0.01; ***, P<0.001. Error bars, 68% confidence intervals estimated by a bootstrapping procedure (see Methods).

D. Same as A, but for decoding eye of origin. Binning by polar angle does not improve decoding performance compared to random binning in V1, suggesting eye preference (unlike orientation preference) is not organized in a large-scale radial pattern.

E. Effect of binning by eccentricity on orientation decoding. Binning by eccentricity does not improve decoding performance relative to random binning, indicating that orientation

preference does not show a large-scale eccentricity bias.
F. Same as D, but for decoding eye of origin. Binning by eccentricity does not improve performance for decoding eye-of-origin relative to random binning, suggesting that the distribution of eye preference is not systematically related to eccentricity.

Figure 5. Effect of binning by visual hemifield on classification performance for decoding orientation and eye-of-origin in V1-V3. Plot symbols, error bars, and conventions as in Figure 5.
A-C. Binning by hemifield significantly improves classification performance for decoding orientation in all areas, except V3 for cardinal orientations.
D-F. Binning by visual hemifield significantly improves decoding performance for eye-of-origin compared to random binning for both stimulus orientations in V1, and for at least one orientation in V2 and V3, consistent with a large-scale left-right hemifield organization in eye preference.

Figure 6. Effect of regressing out large-scale spatial patterns on decoding performance.as function of voxel inclusion threshold (R^2).
A-C. Regressing out angular position significantly reduces decoding performance for orientation in V1-V3. Classification performance (proportion reduction in error) for decoding stimulus orientation (averaged across cardinal and oblique orientations) in areas V1-V3 as a function of voxel inclusion threshold (R^2). *Filled symbols:* Decoding performance computed on data with polar angle component removed. *Open symbols:* Decoding performance on original data. P-values indicate significance of difference between thresholds (computed using a resampling procedure, see Methods). Error bars, standard error of the mean across subjects.
D-F. Regressing out visual hemifield significantly reduces decoding performance for eye-of-origin in V1 and V2, but not V3. Plot symbols, error bars and conventions as in A-C.

Figure 7. Effect of spatial filtering of voxel responses on decoding performance.
A-C. Decoding performance for orientation in V1-V3 as a function of lowpass (filled symbols) and highpass (open symbols) filter size. Error bars, standard error of the mean across subjects. **D-F.** Same as panels A-C but for decoding eye-of-origin.

Figure 8. Orientation and eye preference patterns in V2 and V3 are significantly correlated

with patterns of V1 stimulus preference.

A-B. Eye and orientation preference in V2 as a function of eye preference in V1. Each plot symbol corresponds to the stimulus preference (t-value of contrast between right and left eye stimulation, data collapsed across stimulus orientations) of a single voxel in V2 plotted against V1 stimulus preference at the corresponding visual field location. Different plot symbols represent different subjects; size of each plot symbol indicates goodness-of-fit of voxel time series (R^2). The spatial patterns of both eye and orientation preferences in V2 are significantly correlated with V1 eye and orientation preference patterns respectively.

C. Average correlation (Pearson) between V1 and V2/V3 stimulus preference patterns. Error bars, standard error of the mean across subjects.

D, E. Binning by V1 eye preference significantly improves decoding performance for eye-of-origin compared to random binning in V2 and V3.

F. Binning by V1 orientation preference significantly improves decoding performance for orientation compared to random binning in V2 and V3.

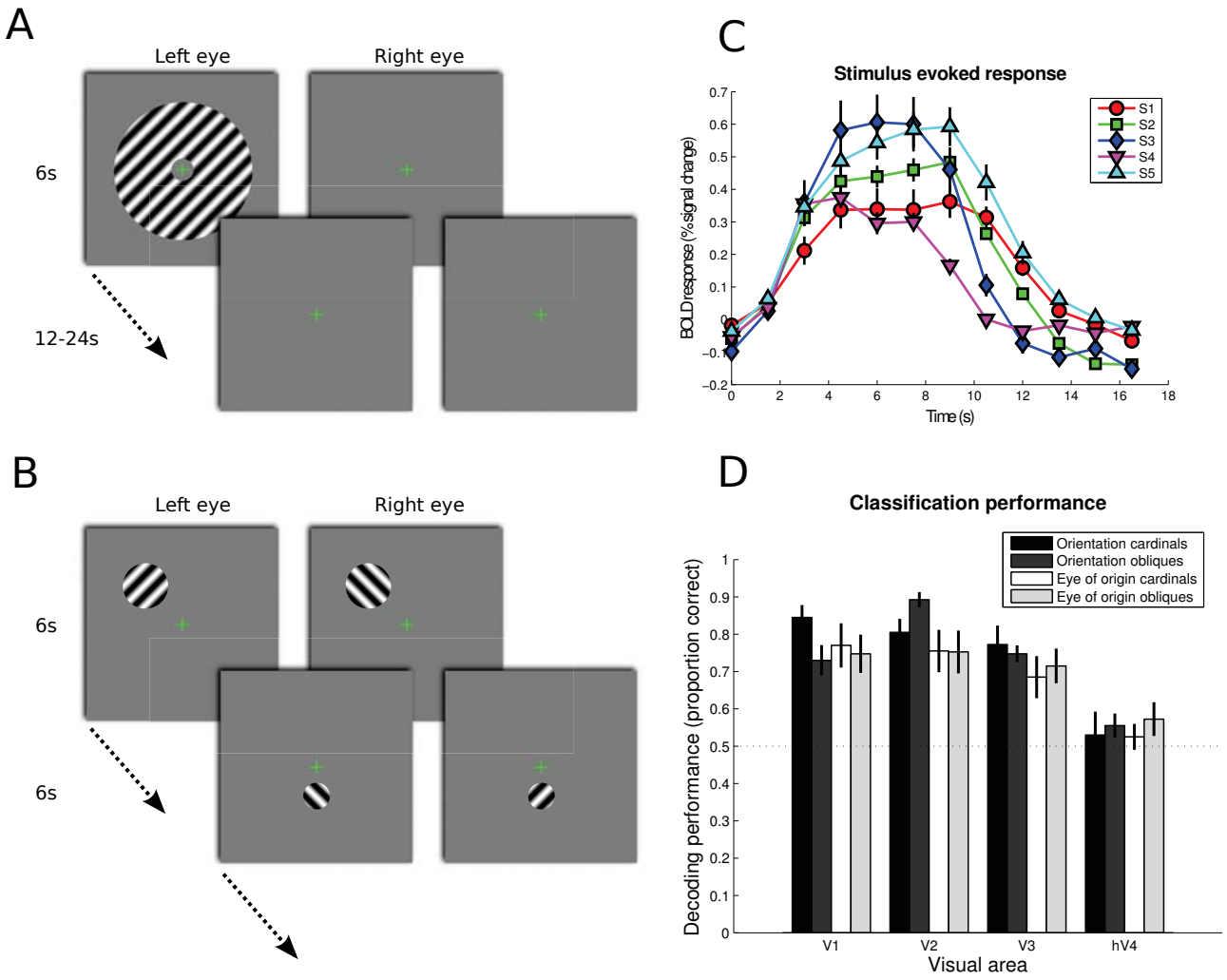
A
Left eye
Right eye
6s
12-24s
B
Left eye
Right eye
6s
6s
C
Stimulus evoked response
S1
S2
S3
S4
S5
BOLD response (%signal change)
Time (s)
D
Classification performance
Orientation cardinals
Orientation obliques
Eye of origin cardinals
Eye of origin obliques
Decoding performance (proportion correct)
V1
V2
V3
hV4
Visual area

Figure 1

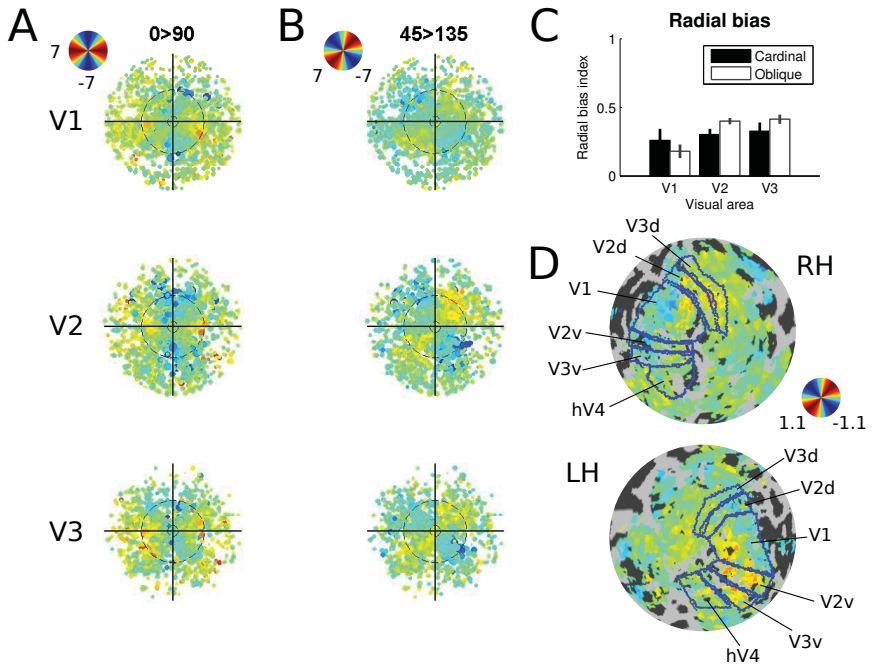
A
0>90
7
-7
V1
V2
V3
B
45>135
7
-7
C
Radial bias
Cardinal
Oblique
Radial bias index
1
0.5
0
V1
V2
V3
Visual area
D
RH
V3d
V2d
V1
V2v
V3v
hV4
1.1
-1.1
LH
V3d
V2d
V1
V2v
V3v
hV4

Figure 2

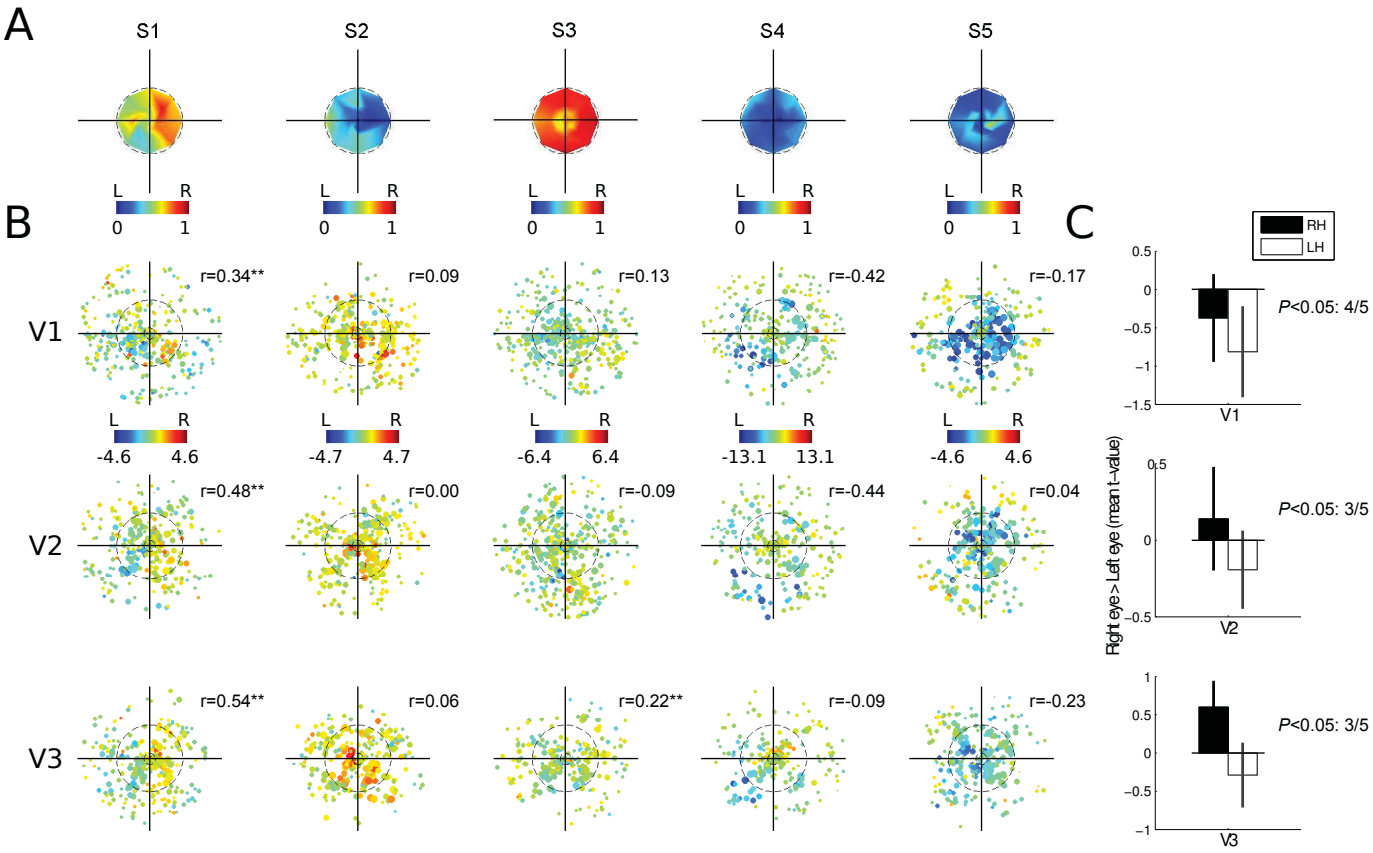
A
S1
S2
S3
S4
S5
L
R
0
1
B
V1
V2
V3
r=0.34**
r=0.09
r=0.13
r=-0.42
r=-0.17
-4.6
4.6
-4.7
4.7
-6.4
6.4
-13.1
13.1
r=0.48**
r=0.00
r=-0.09
r=-0.44
r=0.04
r=0.54**
r=0.06
r=0.22**
r=-0.09
r=-0.23
C
RH
LH
P<0.05: 4/5
P<0.05: 3/5
P<0.05: 3/5
Right eye>Left eye (mean t-value)

Figure 3

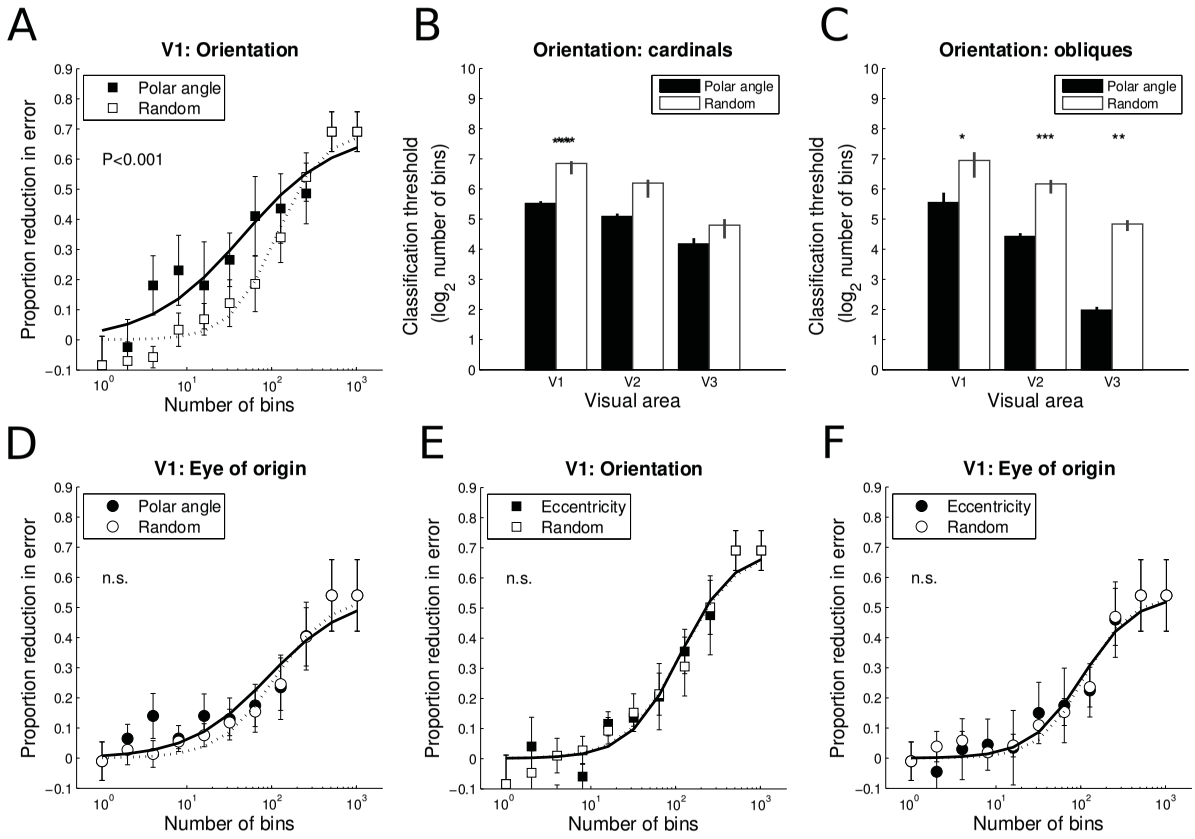
A
V1: Orientation
Polar angle
Random
P<0.001
Proportion reduction in error
Number of bins
B
Orientation: cardinals
Polar angle
Random
****
Classification threshold
(log2 number of bins)
V1
V2
V3
Visual area
C
Orientation: obliques
Polar angle
Random
*
***
**
Classification threshold
(log2 number of bins)
V1
V2
V3
Visual area
D
V1: Eye of origin
Polar angle
Random
n.s.
Proportion reduction in error
Number of bins
E
V1: Orientation
Eccentricity
Random
n.s.
Proportion reduction in error
Number of bins
F
V1: Eye of origin
Eccentricity
Random
n.s.
Proportion reduction in error
Number of bins

Figure 4

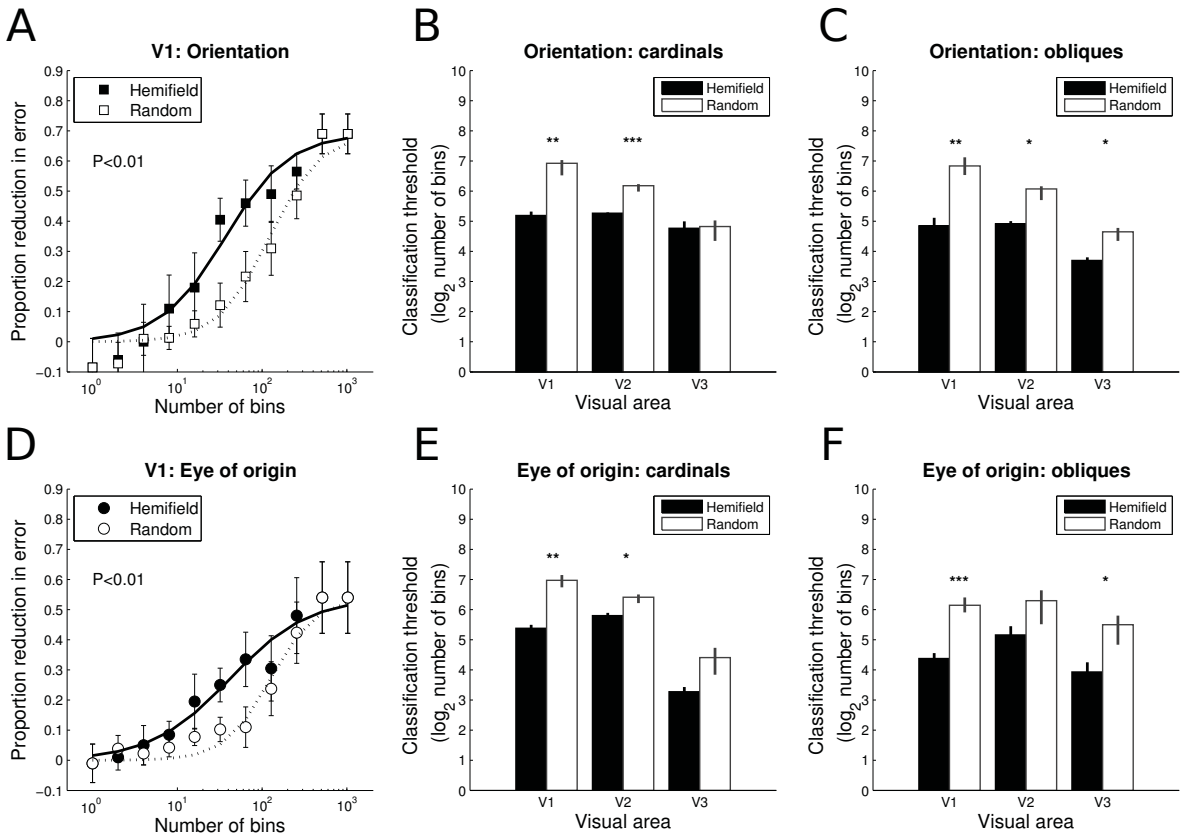
A
V1: Orientation
Hemifield
Random
P<0.01
Proportion reduction in error
Number of bins
B
Orientation: cardinals
Classification threshold (log2 number of bins)
Visual area
V1
V2
V3
C
Orientation: obliques
D
V1: Eye of origin
E
Eye of origin: cardinals
F
Eye of origin: obliques

Figure 5

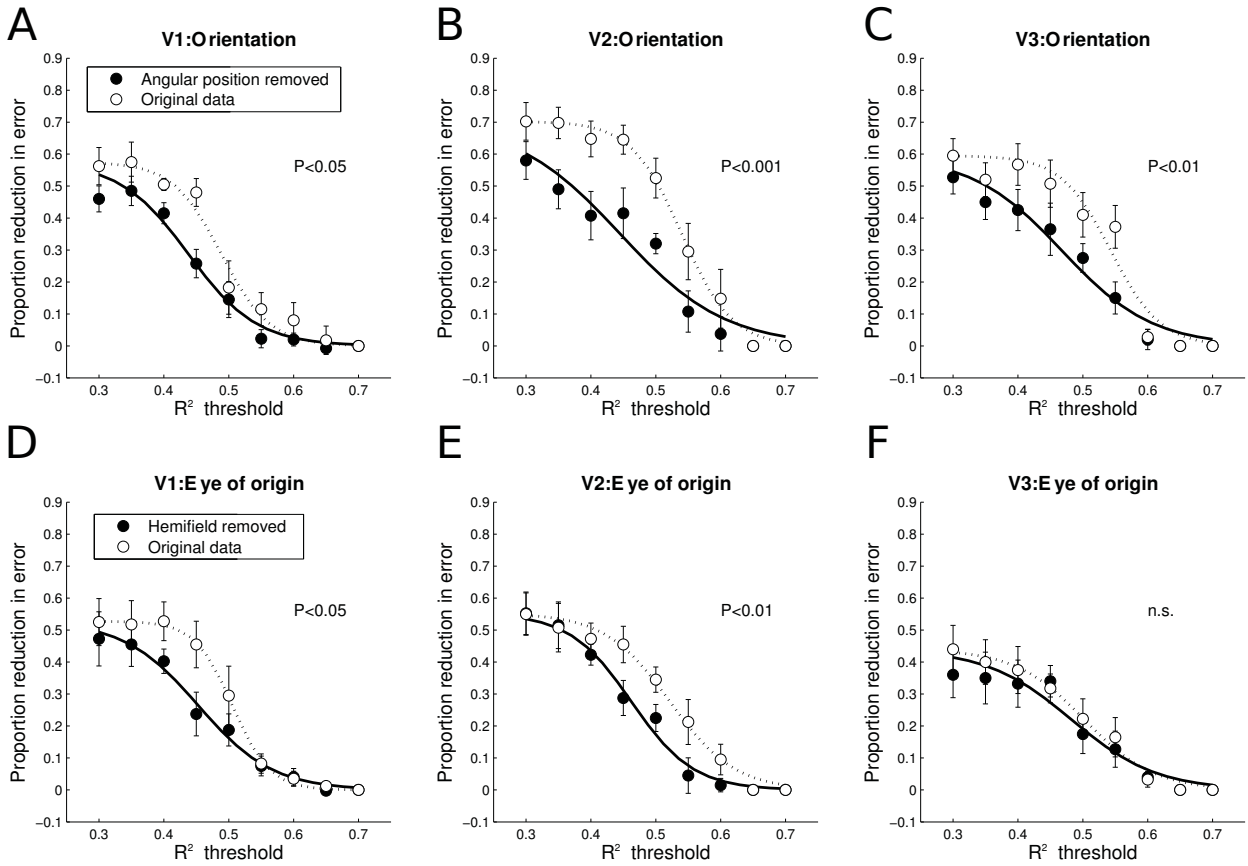
A
V1:Orientation
Angular position removed
Original data
P<0.05
B
V2:Orientation
P<0.001
C
V3:Orientation
P<0.01
D
V1:Eye of origin
Hemifield removed
Original data
P<0.05
E
V2:Eye of origin
P<0.01
F
V3:Eye of origin
n.s.
Proportion reduction in error
R² threshold

Figure 6

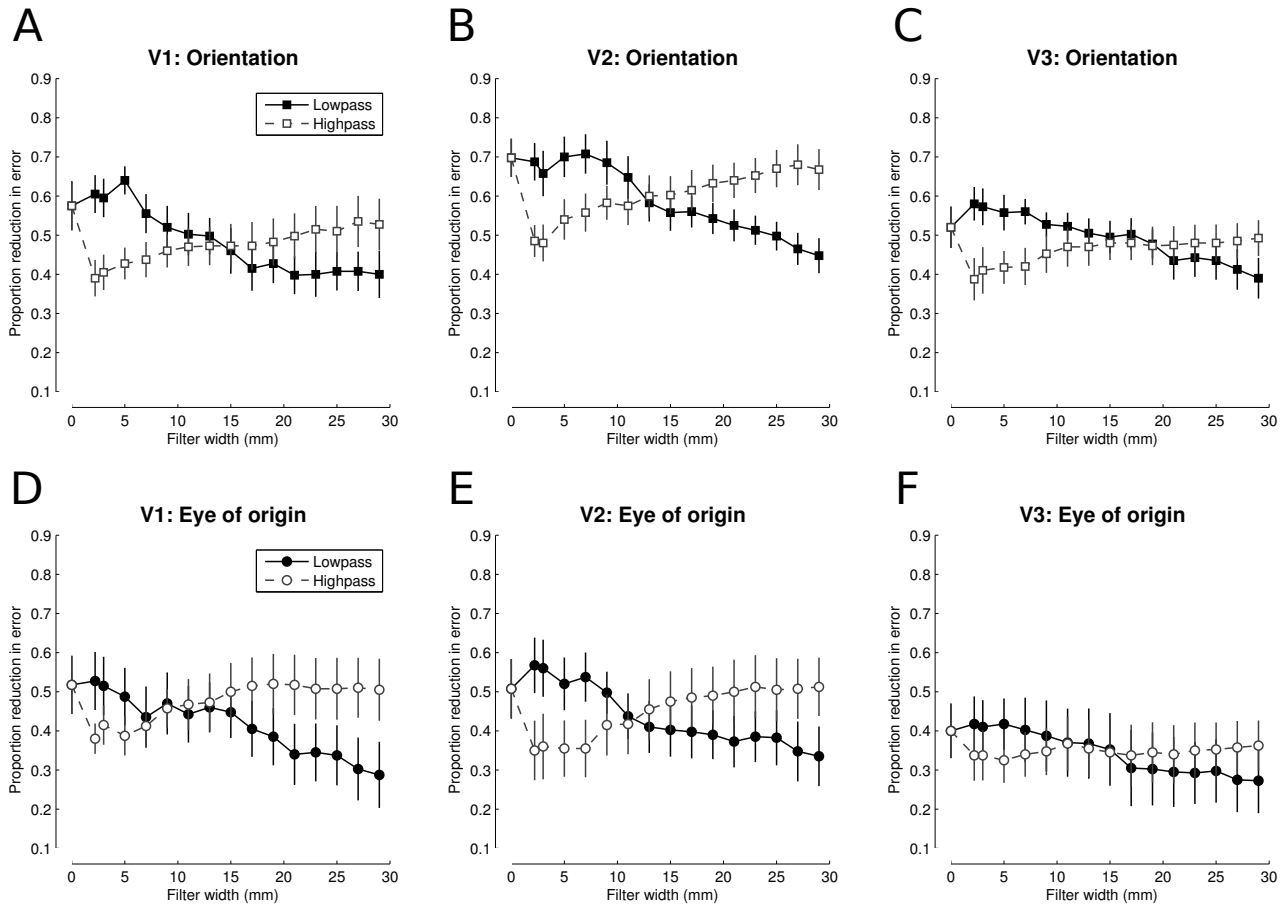
A
V1: Orientation
B
V2: Orientation
C
V3: Orientation
D
V1: Eye of origin
E
V2: Eye of origin
F
V3: Eye of origin
Lowpass
Highpass
Proportion reduction in error
Filter width (mm)

Figure 7

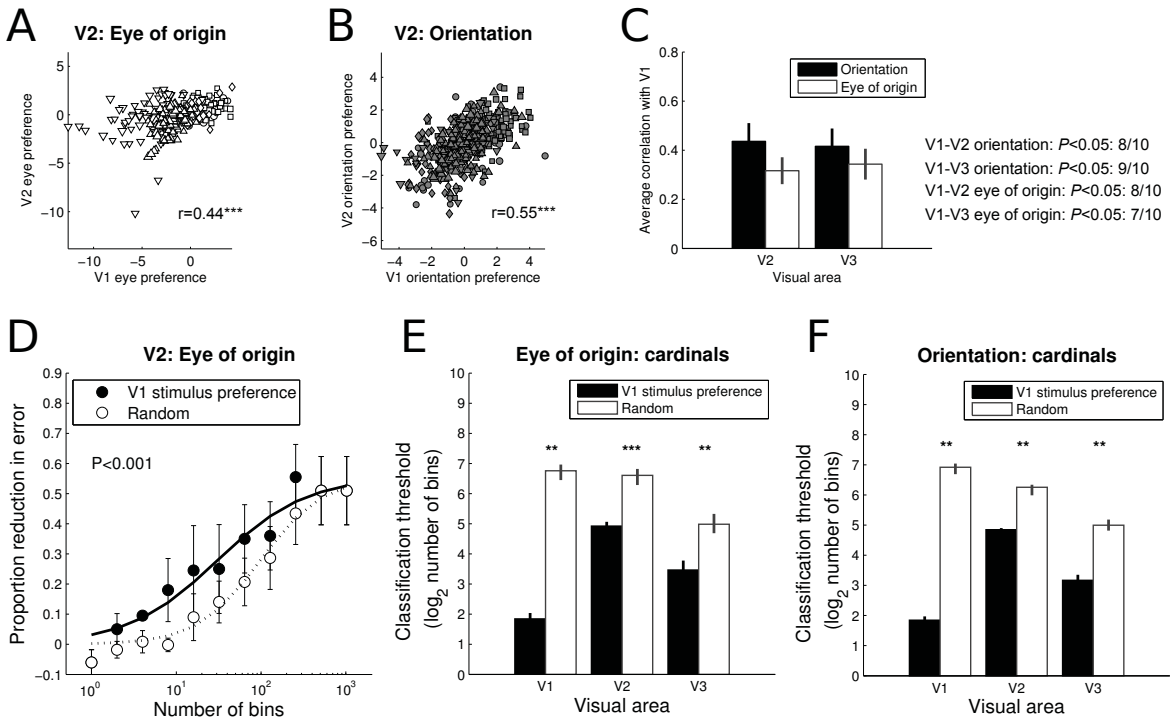
A
V2: Eye of origin
V2 eye preference
V1 eye preference
r=0.44***
B
V2: Orientation
V2 orientation preference
V1 orientation preference
r=0.55***
C
Orientation
Eye of origin
Average correlation with V1
Visual area
V1-V2 orientation: P<0.05: 8/10
V1-V3 orientation: P<0.05: 9/10
V1-V2 eye of origin: P<0.05: 8/10
V1-V3 eye of origin: P<0.05: 7/10
D
V2: Eye of origin
V1 stimulus preference
Random
P<0.001
Proportion reduction in error
Number of bins
E
Eye of origin: cardinals
V1 stimulus preference
Random
Classification threshold (log2 number of bins)
Visual area
F
Orientation: cardinals
V1 stimulus preference
Random
Classification threshold (log2 number of bins)
Visual area

Figure 8